

Oceanographic Processes Driving Low Oxygen Conditions Favoring Deoxygenation Inside Patagonian Fjords

Pamela Linford^{1,2}, Iván Pérez-Santos^{2,3,4,*}, Paulina Montero^{3,4}, Patricio Díaz^{2,5}, Claudia Aracena^{6,7}, Elías Pinilla^{8,13,4}, Facundo Barrera^{2,9,10}, Manuel Castillo¹¹, Aida Alvera-Azcárate¹², Mónica Alvarado¹³, Gabriel Soto⁸, Cécile Pujol¹², Camila Schwerter², Sara Arenas-Urbe², Pilar Navarro², Guido Mancilla-Gutiérrez², Robinson Altamirano², Javiera San Martín^{8,7}, Camila Soto-Riquelme⁸.

¹Programa de Doctorado en Ciencias, Mención Conservación y Manejo de Recursos Naturales, Universidad de Los Lagos, Puerto Montt, Chile.

²Centro i-mar, Universidad de Los Lagos, Casilla 557, Puerto Montt, Chile.

³Center for Oceanographic Research COPAS Sur-Austral and COPAS COASTAL, Universidad de Concepción, Chile.

⁴Centro de Investigación en Ecosistemas de la Patagonia (CIEP), Coyhaique, Chile.

⁵CeBiB, Universidad de Los Lagos, Casilla 557, Puerto Montt, Chile.

⁶Centro de Investigación en Recursos Naturales y Sustentabilidad, Universidad Bernardo O'Higgins, Avenida Viel 1497, Santiago, Chile.

⁷Laboratorio Costero de Recursos Acuáticos de Calfuco, Universidad Austral de Chile, Valdivia, Chile.

⁸Instituto de Fomento Pesquero (IFOP), CTPA-Putemún, Castro, Chile.

⁹Fundación Bariloche and CONICET, San Carlos de Bariloche, Argentina Centro de Ciencia del Clima y la Resiliencia (CR2), Universidad de Chile, Chile.

¹⁰Centro Austral de Investigaciones Científicas (CADIC), CONICET, Bernardo Houssay 200, Ushuaia, Argentina.

¹¹Centro de Observación Marino para estudios de riesgos del ambiente Costero, Universidad de Valparaíso Valparaíso, Chile.

¹²AGO-GHER, University of Liège, Belgium.

¹³Servicio Hidrográfico y Oceanográfico de la Armada de Chile.

¹⁴Department of Civil and Environmental Engineering, University of Maine, 5711 Boardman Hall, Orono, ME, USA.

Correspondence to: I. Pérez-Santos (ivan.perez@ulagos.cl), <https://orcid.org/0000-0002-0184-1122>.

Abstract

The dissolved oxygen (DO) levels of oceanic-coastal waters has decreased over the last decades owing to the increase in surface and subsurface water temperature caused by climate change. In addition, biological and human

activity in coastal zones, bays, and estuaries has contributed to the acceleration of current [oxygen loss/deoxygenation](#). The Patagonian fjord and channel system is one world region where low DO water (LDOW, 30%–60% oxygen saturation) and hypoxia conditions (<30% oxygen saturation, 2 ml L⁻¹ or 89.2 μmol L⁻¹) is observed. An *in-situ* data set of hydrographic and biogeochemical [parameters–variables \(2017–1507 stations\)](#), collected from sporadic oceanographic cruises between 1970 and 2021, was used to [evaluate/quantify](#) the mechanisms involved in the presence of LDOW and hypoxic conditions in northern Patagonian fjords. Results denoted two main areas with LDOW (e.g., Puyuhuapi Fjord-Jacaf channel, Comau Fjord, and the Reloncaví estuarine system) extending from 25–400 m depth. Simultaneously, hypoxia was recorded in the Puyuhuapi Fjord, Jacaf Channel, and Quitalco Fjord. Quitalco registered the lowest values of DO (9.36 μmol L⁻¹ and 1.6% oxygen saturation) of the entire Patagonian fjord system. Areas of LDOW and hypoxia coincided with the accumulation of inorganic nutrients. Water mass analysis confirmed the contribution of equatorial subsurface water in the advection of the LDOW to only the Puyuhuapi Fjord and Jacaf Channel. In addition, in Puyuhuapi Fjord, hypoxic conditions occurred when the community respiration rate (6.6 g C m⁻²d⁻¹) exceeded the gross primary production estimate (1.9 g C m⁻²d⁻¹) possibly due to the increased consumption of DO during the use of both autochthonous and allochthonous organic matter. ~~Biogeochemical processes and circulation regimens also contribute to deoxygenation and will be part of the discussion of the present research. This study elucidates the physical and biogeochemical processes contributing to hypoxia and LDOW in the northern Patagonian fjords, highlighting the significance of performing multidisciplinary research and applying of numerical model.~~

1 Introduction

Hypoxic conditions and ~~low dissolved oxygen water (LDOW) deoxygenation~~ have expanded globally over the last decade along coastal [waterszones](#) and oceans (Schmidtke et al., 2017; Breitburg et al., 2018). While hypoxia is mostly attributed to anthropogenic processes, such as eutrophication (Díaz et al., 2001; Conley et al., 2009; Meire et al., 2013), ~~LDOW and deoxygenation~~ occurs most prominently in the open ocean ~~as a combination due to of~~ natural ~~and anthropogenic~~ forcing (Oschlies et al., 2018; Garçon et al., 2019). ~~However, the trend of deoxygenation has recently accelerated owing to the warming of oceans due to climate change.~~ Therefore, for decades, the scientific community has been paying close attention to this issue because of the expected impacts on the survival, abundance, development, growth, reproduction, and behavior of the most important taxonomic groups at different stages of their life cycles, such as mollusks, crustaceans, and fish (Sampaio et al., 2021, Ekau et al., 2010; Batiuk et al., 2009; Vaquer-Sunyer y Duarte, 2008; Breitburg et al., 1997; Díaz ~~y~~ and Rosenberg, 1995; Andrewartha and Birch, 1986; Davis, 1975), which could also affect all services provided to humans (Laffoley and Baxter, 2019).

Some examples of the impact of LDOW on biological behaviors are changes in the composition of benthic communities in prolonged periods of DO<4.2 ml L⁻¹ (Hoos, 1973); negative impact on the growth and abundance of cod (3.6 ml L⁻¹; 70%), the limit of the distribution of sardine larvae (2.6 ml L⁻¹; 50%), the distribution of jellyfish (1.6 ml L⁻¹; 30%), the decrease of the abundance, swimming capacity and filtration of copepods (0.52 ml L⁻¹; 10%), described by Ekau et al., (2010). Additionally, oxygen deficiency affects the growth rate and feed conversion efficiency, and in some species, even increases the concentration of toxic substances (Davis, 1975). In a Patagonian

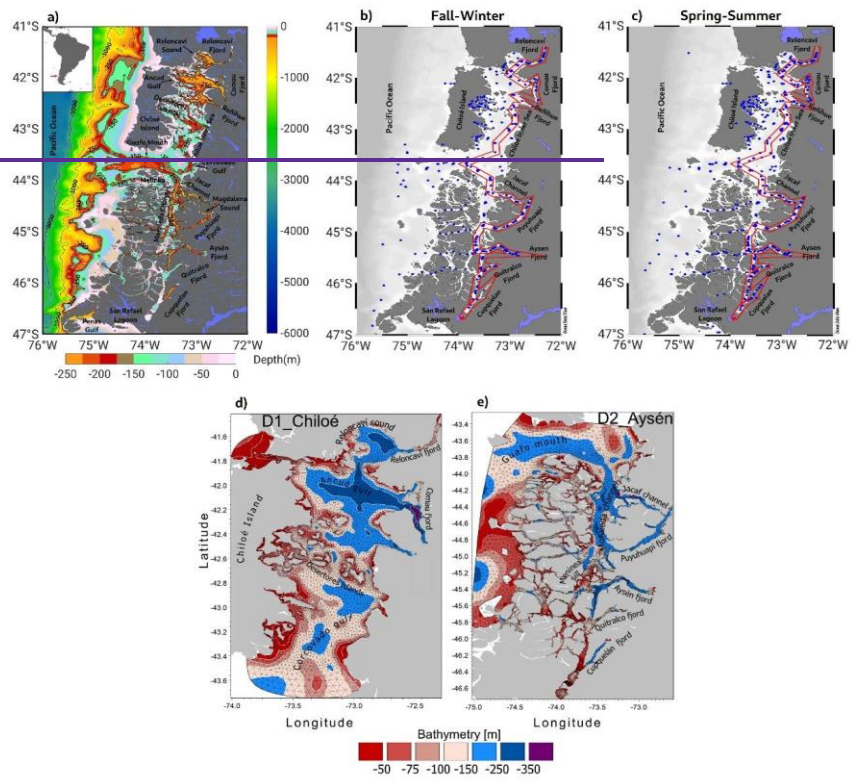
fjord used for recreational fishing for rainbow trout (*Salmo gairdneri*) used in recreational fishing, values less than under 50% saturation caused a reduction in swimming speed (Jones, 1971b) and altered respiration and metabolism (Kutty, 1968a). In the case of coho salmon (*Oncorhynchus kisutch*), a commonly farmed species, a growth rate proportional to the oxygen level was observed for saturations between 40% and 80% (Herrmann, 1958), and the hypoxia modulated the transcriptional immunological response (Martinez et al., 2020). Finally, Pérez-Santos et al. (2018) reported habitat reduction of microzooplankton in a Patagonian fjord (Puyuhuapi Fjord) due to the presence of hypoxic conditions at depths below 100 m.

Throughout the world's oceans, there are areas in which the dissolved oxygen (DO) is significantly lower than in well-oxygenated areas (such as $<20 \mu\text{M}$, $\sim 0.4 \text{ mg L}^{-1}$, or 0.31 ml L^{-1} as shown by Breitburg et al., (2018). These areas are known as oxygen minimum zones (OMZs). ~~Because of the upwelling associated with OMZs, which draws up nutrient rich waters, they experience elevated surface primary production.~~ OMZs result from organic matter degradation, weak water circulation, long residence times, and weak ventilation (Fuenzalida et al., 2009). The major ocean OMZs are located in the Eastern South Pacific, the Arabian Sea, the Bay of Bengal (Indian Ocean), the West Bering Sea, and the Gulf of Alaska, covering approximately 8% of the total ocean or approximately 30 million km^2 (Paulmier and Ruiz-Pino, 2009; Fuenzalida et al., 2009).

Along the Perú-Chile coastline, the Eastern South Pacific (ESP) OMZ extends poleward, ~~decreasing in strength and size to the south near the Patagonian fjord system diminishing its influence on the adjacent coast of the Patagonian fjord system~~ (Silva et al., 2009). Recently, Linford et al. (2023) demonstrated poleward transport of hypoxic and LDOW of the Equatorial Subsurface water mass (ESSW) alongside the Patagonian region. As ESSW (originated in the Equatorial region) moves south, it passes throughout the OMZ, carrying oxygen-poor water ($2\text{--}3 \text{ ml L}^{-1}$) with high nitrate concentration ($20\text{--}30 \mu\text{M}$) and elevated salinity (34.9) (Silva et al., 2009). Studies of water masses inside Patagonian fjords and channels have detected the presence of ESSW only in the northern region, between 41° S and 45° S . This water mass enters the northern Patagonia region via the Guafo mouth (Figure 1b), a deep channel with a depth of $150\text{--}200 \text{ m}$ and width of 35 km (Sievers and Silva, 2008; Pérez-Santos et al., 2014; Schneider et al., 2014). ESSW is one of the main causes of hypoxia and LDOW inside Patagonian fjords (e.g., Puyuhuapi Fjord and Jacaf Channel). Nevertheless, these conditions are also found in other areas ~~where sills block the pass far from the influence~~ of ESSW, e.g., the Reloncaví system (Reloncaví Fjord and Reloncaví Sound), Aysén, Comau, and Quitrarco fjords (Figure 1) (Silva and Vargas, 2014; Linford et al., 2023; Díaz et al., 2023).

Regarding other processes favoring hypoxia and LDOW inside Patagonian fjords, Silva (2008) proposed those biological processes that include the consumption of DO, such as respiration and the remineralization of organic matter. A high load of organic matter (autochthonous and allochthonous) in the water column and sediments increases DO consumption during microbial community respiration, contributing to the LDOW content in most of the Patagonian fjord headwaters (Castillo et al., 2016) as well as higher community respiration rates than primary production (Montero et al., 2011; Montero et al., 2017a). Weak deep ventilation and long residence times in fjord waters are also assumed to promote a reduction in the DO concentration (Schneider et al., 2014; Silva and Vargas, 2014).

110 Finally, most published manuscripts hypothesize and discuss the processes favoring hypoxia and LDOW
deoxygenation inside Patagonian fjords without but never showing any evidence, particularly that based on g in-situ
data and fieldwork experiments-quantification. The Patagonian fjords ecosystem is under substantial continued
economic pressure due to, with, salmon aquaculture and other economic activities occupying the first position, with
a national production of ~1,000,000 tons of salmon in 2019 (Billi et al., 2022). The northern Patagonian fjords (a
115 region similar to the study area; Figure 1b, 1c) reported half of the national production and a significant number of
salmon concessions (Billi et al., 2022). A risk analysis carried out in this region established that the Reloncaví
estuarine system, and the Comau, Puyuhuapi, Quitalco, and Cupquelan fjords are regions with an especially
elevated level of risk for the development of harmful algal blooms (HABs) and eutrophication events, owing to the
nutrients input by the intense aquaculture of salmon (Soto et al., 2021). Nevertheless, environmental studies on
salmon farming have shown that this economic activity has a geographically limited impact, because most nutrients
120 are quickly recycled by biological processes in the water column (Soto and Norambuena, 2004).



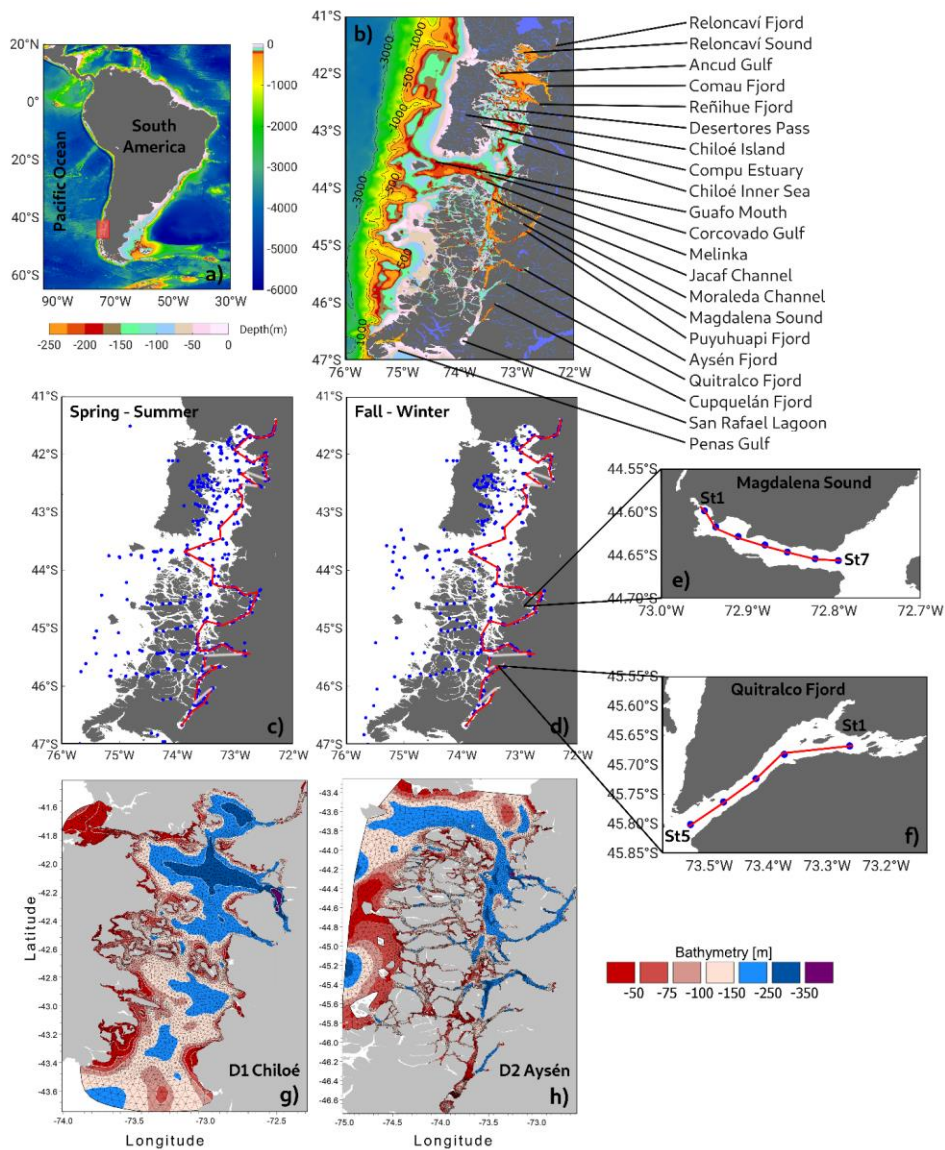


Figure 1. (a) Map showing the study area in the (b) northern region of Patagonian fjords. Color bars represent bathymetric features from ETOPO2. (bc, ed) Sampling stations during the spring-summer and fall-winter and spring-summer seasons. Red lines in (bc, ed) represent along-fjord transects carried out to describe vertical features of hydrographic-biogeochemical stations from Figure 2, 4, and 5. Data was collected on sporadic cruises, from

1970–2021 (see Table 1). [\(e, f\) Details of Magdalena Sound and Quitralco Fjord sampling stations.](#) [\(dg, eh\)](#) High-resolution model domain includes the northern Patagonia inner sea and is denoted as D1_Chiloé, while D2_Aysén covers the southern section. Bathymetry used was based on an SHOA nautical chart from the Chilean Navy.

Another meaningful impact of salmon production is the increase in allochthonous organic matter load, which, when combined with the high production of autochthonous organic matter by phytoplankton, favors a decrease in DO in the water column and sediments (Quiñones et al., 2019). Salmon farming supplies allochthonous dissolved substrates through the dissolution of organic particles derived from feces and uneaten feed (Wang et al., 2012). This organic material is considered highly degradable (Nimptsch et al., 2015; Montero et al., 2022), promoting enhanced rates of heterotrophic bacterial activity (e.g., bacterial production (BP) and extracellular enzymatic activity (EEA) (Montero et al., 2022).

The main goal of this study was to [analyze-quantify](#) the processes contributing to hypoxia and LDOW in northern Patagonia, such as ESSW advection, DO consumption during the use of organic matter (community respiration), biogeochemical processes, deep-water ventilation, and residence times of water inside fjords. An *in-situ* dataset of ~2000 profilers of hydrographic-chemical [parameters-variables](#) was used to describe the seasonal distribution of water masses and their relationship with biogeochemical processes. Primary production experiments and the output of a 3D hydrodynamic model were utilized to demonstrate the occurrence of other processes [promoting low oxygen conditions involved](#) in the [deoxygenation-of-the](#) northern Patagonian fjords.

2. Materials and Methods

2.1 Hydrographic and chemical data

A total of [15072017](#) stations were used to describe northern Patagonia's hydrographical and chemical processes; 593 stations were sampled during the fall-winter seasons and [9144424](#) during the spring-summer seasons (Table 1). Most temperature and salinity records were obtained using a CTD (Conductivity, Temperature, and Depth profiler) instrument (e.g., SBE19 plus, SBE15, and AML Metrec XL). [When SEB CTDs were used, data were processed according to the manufacturer's protocol and software \(SBE Data Processing\). When using AML CTD, the raw data underwent a quality control, eliminating records out of range according to historical CTD data \(Pérez-Santos et al., 2014; Pérez-Santos et al., 2021; Linford et al., 2023\), after which the data were averaged every 1 m. Additionally, membrane and Optical-optical sensors \(e.g., SBE 43 and Optode 4831\) together with and the Winkler method have been used to obtain DO data \(Strickland and Parsons, 1968\). Experiments were conducted to validate the CTD-DO data with the Winkler method showing satisfactory results and high statistical correlation \(\$R^2\$ ranging 0.92–0.99, Figure not included\).](#)

Figures 1b and 1c show the station positions during fall-winter and spring-summer. The absolute salinity (S_A in gkg^{-1}) and conservative temperature (θ in $^{\circ}\text{C}$) were calculated using the Thermodynamic Equation of Seawater 2010 (TEOS-10) (IOC et al., 2010). In TEOS-10, absolute salinity represents the spatial variation in the composition of seawater, considering the different thermodynamic properties and gradients of horizontal density in

the open ocean. Conservative temperature is similar to potential temperature but represents the heat content of seawater with greater precision.

A temperature/salinity (TS) diagram was constructed based on the conservative temperature and absolute salinity values, which was used to identify and quantify the water masses in the Patagonian fjords using only the salinity criteria proposed by Sievers (2008) and Sievers and Silva (2008). According to this classification, Estuarine Water (EW, 0–1 g kg⁻¹) was detected in the surface layer owing to the water supply from rivers and summer time glacier melting. Below the EW, a Modified Subantarctic Water (MSAAW) layer was found, with salinities values ranging 31–33 g kg⁻¹. The MSAAW originated from mixing of the EW and Subantarctic Water (SAAW, salinity 33–33.8 g kg⁻¹). Finally, an Equatorial Subsurface Water (ESSW) layer was identified, with salinity values higher than 33.8 g kg⁻¹. The ESSW was localized near the bottom of the Puyuhuapi Fjord and Jacaf Channel (Linford et al., 2023).

The long-term seasonal means were calculated using the Data Interpolation Variational Analysis (DIVA) gridding software developed by the University of Liege (<http://modb.oce.ulg.ac.be/mediawiki/index.php/DIVA>). The DIVA software was used to analyze and interpolate datasets via an optimal interpolation method, which considers the coastline and bathymetry of the study area; the calculations were executed on a finite element mesh adapted to the gridding domains (Troupin et al., 2010). Additionally, the DIVA results were graphically displayed using the Ocean Data View software (<https://odv.awi.de>).

Table 1. Oceanographic campaigns carried out in Patagonian fjords and channels.

Expeditions	Date	Season	Stations	Measurements
HUDSON	06/03-01/04, 1970	Summer	112	(Temperature, Salinity) [*] + O ₂ (bottle-Winkler) + Nutrients (PO ₄ , NO ₃ , Si; bottle)
CIMAR-01	18/10-04/11, 1995	Spring	99	CTD + O ₂ (bottle-Winkler) + Nutrients (PO ₄ , NO ₃ , NO ₂ , Si; bottle) + pH(bottle)
CIMAR-02	16/10-17/11, 1996	Spring	101	CTD + O₂(bottle-Winkler) + Nutrients (PO₄, NO₃, Si; bottle) + pH(bottle)
CIMAR-04-I	28/09-09/10, 1998	Spring	31	CTD + O ₂ (bottle-Winkler) + Nutrients (PO ₄ , NO ₃ , Si; bottle)
CIMAR-03	11-22/10/1998	Spring	59	CTD + O₂(bottle-Winkler) + Nutrients (PO₄, NO₃, Si; bottle)
CIMAR-07-I	07-21/07/2001	Winter	49	CTD + O ₂ (bottle-Winkler)
CIMAR-07-II	13-25/11/2001	Spring	51	CTD + O ₂ (bottle-Winkler) + Nutrients (PO ₄ , NO ₃ , Si; bottle)
CIMAR-08-I	06-20/07/2002	Winter	51	CTD + O ₂ (bottle-Winkler) + Nutrients (PO ₄ , NO ₃ , Si; bottle)
CIMAR-08-II	16-24/11/2002	Spring	39	CTD + O ₂ (bottle-Winkler) + Nutrients (PO ₄ , NO ₃ , Si; bottle)
CIMAR-09-I	09-23/08/2003	Winter	58	CTD + O ₂ (bottle-Winkler) + Nutrients (PO ₄ , NO ₃ , Si; bottle)
CIMAR-09-II	07-20/11/2003	Spring	55	CTD + O ₂ (bottle-Winkler) + Nutrients (PO ₄ , NO ₃ , Si; bottle)
CIMAR-10-I	26/06-31/08, 2004	Winter	49	CTD + O ₂ (bottle-Winkler) + Nutrients (PO ₄ , NO ₃ , Si; bottle)

CIMAR-10-II	12-23/11/2004	Spring	63	CTD + O2(bottle-Winkler) + Nutrients (PO4, NO3, Si; bottle)
CIMAR-11-I	18-25/07/2005	Winter	78	CTD + O2(bottle-Winkler) + Nutrients (PO4, NO3, Si; bottle)
CIMAR-11-II	11-21/11/2005	Spring	80	CTD + O2(bottle-Winkler) + Nutrients (PO4, NO3, Si; bottle)
CIMAR-12-I	10-19/07/2006	Winter	32	CTD + O2(bottle-Winkler) + Nutrients (PO4, NO3, Si; bottle)
CIMAR-12-II	04-12/11/2006	Spring	40	CTD + O2(bottle-Winkler) + Nutrients (PO4, NO3, Si; bottle)
CIMAR-13-I	27/07-07/08, 2007	Winter	42	CTD + O2(bottle-Winkler) + Nutrients (PO4, NO3, Si; bottle)
CIMAR-13-II	02-12/11/2007	Spring	46	CTD + O2(bottle-Winkler) + Nutrients (PO4, NO3, Si; bottle)
CIMAR-14	01-19/11/2008	Spring	59	CTD + O2(bottle-Winkler) + Nutrients (PO4, NO3, Si; bottle)
CIMAR-15	09/10-09/11, 2009	Spring	51	CTD + O2(bottle-Winkler) + Nutrients (PO4, NO3, Si; bottle)
CIMAR-16	20/10-12/11, 2010	Spring	122	CTD + O2(bottle-Winkler) + Nutrients (PO4, NO3, Si; bottle)
CIMAR-17	17/10-14/11, 2011	Spring	195	CTD + O2(bottle-Winkler) + Nutrients (PO4, NO3, Si; bottle)
CIMAR-18	01/06-04/07, 2012	Fall-Winter	98	CTD + O2(bottle-Winkler) + Nutrients (PO4, NO3, Si; bottle)
CIMAR-19	04-16/07/2013	Winter	70	CTD + O2(bottle-Winkler) + Nutrients (PO4, NO3, Si; bottle)
CIMAR-20	04-22/10/2014	Spring	81	CTD + O2(bottle-Winkler) + Nutrients (PO4, NO3, Si; bottle)
CHEPU-IFOP	05-17/08/2017	Winter	22	CTD + O2(optic)
CIMAR-23	27/10-15/11, 2017	Spring	37	CTD + O2(optic) + Nutrients (PO4, NO3, Si; bottle)
CIMAR-24	26/09-16/10, 2018	Spring	37	CTD + O2(bottle-Winkler) + Nutrients (NO3; bottle)
CHEPU-MR-I	06-08/06/2018	Fall	12	CTD + O2(optic)
CHEPU-MR-II	11/10/2018	Spring	2	CTD + O2(optic)
PN-I (IFOP)	13-25/11/2020	Spring	32	Fluor (optic)
PN-II (IFOP)	24/02-04/03, 2021	Summer	32	CTD + O2(optic) + Nutrients (PO4, NO3, NO2, Si; bottle) + pH, Chl-a, Tur, -Fluor (optic)
PN-III (IFOP)	28/07-10/08, 2021	Winter	32	CTD + O2(optic) + Nutrients (PO4, NO3, NO2, Si; bottle) + pH, Chl-a, Tur, Fluor (optic)
593 Fall-Winter + 914 424 Spring-Summer = 1507 2017 stations				

**Temperature and salinity were measured with a reversing thermometer and inductive salinometer respectively.*

185

2.2 Primary production, community respiration, bacterial production, and phytoplankton community.

During the spring-summer period of 2020–2021 and summer of 2022, nine *in situ* experiments were conducted to measure gross primary production (GPP) and community respiration (CR) in some fjords of northern Patagonia (Table 2). Water samples were obtained from three depths (2, 10, and 20 m depth) at each sampling station. GPP and CR rates were estimated from changes in dissolved oxygen concentrations observed during *in situ* incubation of light and dark bottles (Strickland, 1960). Water from the Niskin bottles was transferred into 125 mL

190

(nominal volume) borosilicate bottles (gravimetrically calibrated) using a silicone tube. Five time-zero bottles, five light bottles, and five dark bottles were used at each incubation depth. Water samples were collected at dawn and incubated throughout the entire light period (approximately ~8–9 h). Time-zero bottles were fixed at the beginning of each experiment, whereas the light and dark incubation bottles were attached to the surface-tethered mooring system. The samples were incubated at the depths from which they were collected.

Dissolved oxygen concentrations were determined according to the Winkler method (Strickland and Parsons, 1968), using an automatic Metrohm burette (Dosimat plus 865) and automatic end-point detection (AULOX Measurement System). Daily GPP and CR rates were calculated as follows: GPP = (mean [O₂] light bottles – mean [O₂] dark bottles); CR = (mean [O₂] time zero bottles – mean [O₂] dark bottles). The GPP and CR values were converted from oxygen to carbon units using a conservative photosynthetic quotient of 1.25 (Williams and Robertson, 1991) and a respiratory quotient of 1.

A total of five bacterial production (BP) experiments were performed during the same period as mentioned above (Table 2). Experiments were conducted using the same water samples collected for the *in situ* GPP and CR incubation experiments. The BP estimates were based on the incorporation of leucine into proteins using the microcentrifugation method (Smith and Azam, 1992). Briefly, a blank and three samples (1.5 mL) were taken from each sampling depth and incubated with L-[3,4,5-³H]-leucine (123.8 Ci mmol⁻¹, 40 nM final concentration) in the dark for 1 h. After incubation, samples were extracted with 100% trichloroacetic acid (TCA), rinsed with 5% TCA, and centrifuged at 13500 rpm twice for 15 min before removal of the supernatant. Liquid scintillation cocktail Ecoscint (1 mL) (National Diagnostic) was added to each sample. The samples were counted for dpm using a Packard (Mod. 1600 TR) liquid scintillation counter. Discrete depth estimates of the GPP, CR, and BS rates were integrated to 20 m using the trapezoidal method.

For analyses of the phytoplankton community, water samples were collected from four discrete depths (2, 4, 10, and 20 m) using a 5 L Niskin bottle. Samples were stored in 120 mL clear plastic bottles and preserved in 1% Lugol's iodine solution (alkaline). From each sample, a 10 mL subsample was placed in a sedimentation chamber and allowed to settle for 12 h (Utermöhl, 1958) prior to identification at 40× and 100× under an inverted microscope (Carl Zeiss, Axio Observer A.1). Finally, taxonomic descriptions from Tomas (1997) were used to identify phytoplankton composition.

Table 2. *In situ* experiments were carried out in Patagonian fjords and channels. Gross primary production (GPP), community respiration (CR), and bacterial secondary production (BSP).

Fjord region	Date (mm-dd-yyyy)	Season	Measurements (g C m ⁻² d ⁻¹)			
			GPP	CR	BSP	GPP:CR
*Reloncaví	02/27/2009	Summer	3.83	3.31	-	1.16
Compu	10/03/2020	Spring	1.22	0.92	0.06	1.32
Quitralco	11/17/2020	Spring	1.41	2.66	0.05	0.53
Camou	12/12/2020	Spring	0.12	1.67	0.15	0.07
Puyuhuapi	01/21/2020	Summer	1.89	6.64	0.25	0.28
Reloncaví	01/14/2021	Summer	2.60	1.90	0.58	1.37
Compu	03/19/2022	Summer	1.25	0.76	-	1.64
Quitralco	02/28/2022	Summer	0.73	1.71	-	0.42

Camou	03/16/2022	Summer	0.56	1.12	-	0.50
Puyuhuapi	01/20/2022	Summer	2.18	2.55	-	0.85

*Data were taken from Montero et al. (2011).

2.3. Satellite images

Sentinel-2 level 1 images were downloaded from the Copernicus Open Access Hub (<https://scihub.copernicus.eu/>) for specific dates and regions, as shown in Table 3. The chosen dates correspond to periods of high discharge of freshwater from the continent. Using ACOLITE v 20220222.0 (<https://odnature.natural-sciences.be/remsem/software-and-data/aeolite>, (Vanhellemont and Rudick, 2018), we calculated suspended particulate matter following Nechad et al. (2016). These data have a spatial resolution of 10 m and allow the resolution of the small-scale distribution of suspended particulate matter within the narrow channels and fjords of the region.

Table 3. Dates and regions of the Sentinel-2 datasets analyzed.

Date	Region
17 March 2017	Puyuhuapi Fjord
09 May 2017	Reloncaví Sound and Fjord
06 April 2018	Comau Fjord
09 June 2022	Quitrileo Fjord

2.3.4 Biogeochemical parameters-variables and analysis

Biogeochemical parameters-variable datas were collected in November 2020 (Expedition PN-I IFOP, Table 1). The water samples were obtained by filtering seawater collected (1–2 L) using a 25-mm diameter, GF/F filter pre-combusted with a (0.7µm pore diameter). Suspended particulate matter (SPM, µg L⁻¹), was determined by gravimetry using the weight difference between the dried filter and the same filter before filtration (Grasshoff et al., 2009). Particulate organic carbon (POC, µmol L⁻¹), total nitrogen (TN, µmol L⁻¹), stable carbon (δ¹³C, ‰) and nitrogen (δ¹⁵N, ‰) isotopes were obtained following the method described by Verardo et al., (1990), with modifications by Barrera et al., (2017) and Díaz et al., (2023), and measured at the Stable Isotope Facility at the Pontifical Catholic University of Chile by using an elemental analyzer (EA Flash 2000 Thermo Finnigan), interfaced to a continuous flow isotope ratio mass spectrometer (IRMS Delta V Advantage).

The stable carbon isotope composition of organic carbon (δ¹³C) can vary depending on its origin, with values ranging from -23 to -19‰ for carbon sources such as marine phytoplankton (Fry and Sherr, 1989; Harmelin-Vivien et al., 2008) and values closer to those of terrestrial organic matter (-30 to -26‰) for other sources (Fry and Sherr, 1989). By analyzing the carbon isotopic composition of organic carbon, it is possible to differentiate carbon between different sources and estimate their contributions. We calculated the relative importance of allochthonous and autochthonous organic matter with two-source endmember mixing models (Bianchi, 2007). Given the fact that the autochthonous marine (f_M) and allochthonous terrestrial fractions (f_T) of organic carbon and nitrogen, respectively, sum to unity according to the importance of autochthonous marine and allochthonous terrestrial fractions were calculated based on the following equation:

255

$$\%POC_{\text{ter}} = \frac{(\delta^{13}C_s - \delta^{13}C_m)}{(\delta^{13}C_t - \delta^{13}C_m)}$$

$$\%POC_{\text{allo}} = \frac{(\delta^{13}C_s - \delta^{13}C_m)}{(\delta^{13}C_t - \delta^{13}C_m)} 100\%$$

260

where $\delta^{13}C_s$ is the isotopic composition of a sample, $\delta^{13}C_m$ is the marine endmember from more oceanic stations (-13.4477 ‰), and $\delta^{13}C_t$ terrestrial is the riverine/lake endmember values for POC (-30.42.933 ‰) as proposed for this area by González et al., (2019). The resulting %POC_{allo} represents the relative contribution of allochthonous (terrestrial) organic carbon to the overall organic carbon pool. Higher values indicate a more significant influence of terrestrial organic carbon, while lower values suggest a higher proportion of autochthonous (marine) organic carbon (González et al., 2019). The carbon: nitrogen ratio was also calculated as a proxy for the organic matter pool (Barrera et al., 2017).

265

Dissolved inorganic nutrients (NO_3^- , NO_2^- , PO_4^{3-} , and Si(OH)_4) were analyzed from 15 mL seawater samples, stored at -20 °C in HDPE bottles, using a Seal AA3 AutoAnalyzer according to the methodology described by Grasshoff et al., (1983) and standard methods for seawater analysis (Kattner and Becker, 1991). Chromophoric Dissolved Organic Matter (CDOM) plays a crucial role in understanding the optical properties and biogeochemical processes in aquatic ecosystems (Stedmon and Nelson, 2015). It is an important component of dissolved organic matter (DOM) that absorbs light in the visible spectrum (ultraviolet and blue wavelengths) and fluoresces at longer wavelengths (Stedmon and Nelson, 2015). CDOM was determined by fluorometry using quinine sulfate dihydrate (μgL^{-1} QSU) diluted in 0.1 N sulfuric acid at a specific wavelength (Ex/Em = 350/450 nm) as standard in a Trilogy Turner Design fluorometer and CDOM module (Kim et al., 2018).

270

2.4.3. Satellite images

275

Sentinel-2 level 1 images were downloaded from the Copernicus Open Access Hub (<https://scihub.copernicus.eu/>) for specific dates and regions, as shown in Table 3. The chosen dates correspond to periods of high discharge of freshwater from the continent. Using ACOLITE v 20220222.0 (<https://odnature.naturalsciences.be/remsem/software-and-data/acolite>, (Vanhellemont and Rudick, 2018), we calculated suspended particulate matter following Nechad et al. (2016). These data have a spatial resolution of 10 m and allow the resolution of the small-scale distribution of suspended particulate matter within the narrow channels and fjords of the region.

280

Table 3. Dates and regions of the Sentinel-2 datasets analyzed.

<u>Date</u>	<u>Region</u>
<u>17 March 2017</u>	<u>Puyuhuapi Fjord</u>
<u>09 May 2017</u>	<u>Reloncaví Sound and Fjord</u>
<u>06 April 2018</u>	<u>Comau Fjord</u>
<u>09 June 2022</u>	<u>Quitralco Fjord</u>

285

2.5 Marine current register with ADCP

In the study region, three mooring systems were deployed in the Corcovado Gulf and Puyuhuapi Fjord (see Figure 9 for position). In each mooring, a Teledyne RD Instruments (TRDI) and a WorkHorse-300 kHz Acoustic Doppler Current Profiler (ADCP) were installed with the transducers facing downward. The instruments were configured with 1-m cell size and 1 h ensembles. The moorings covered the period from January to December 2016, with the ADCP sensors moored between 40 and 100 m. The ADCP provides magnitude and direction (in Earth coordinates); thus, the current vector is decomposed into zonal (u) and meridional (v) components. The basic and standard protocol of quality control was applied to identify outliers and low-quality data following the methodology suggested by TRDI. To obtain the mean pattern of the zonal and meridional components of the currents, they were filtered using a low-pass cosine-Lanzcos filter of 121 weight and 40 h half-power.

2.6 Circulation model

To gain a better understanding of the physical forcing related to the DO dynamics, we used the hydrodynamic model MIKE 3 FM, which solves continuity, momentum, temperature, and salinity transport equations using the finite volume method (DHI, 2019). In this study, two high-resolution model domains include the North Patagonian inner sea named D1 Chiloé (41.3° S– 43.7° S) and D2 Aysén, with an area from 43.6°S to 46.8° S (Figures 1d, 1e). The MIKE 3 model, maintaining the same configuration, has a track record of previous validation and application to investigate the physical aspects of HABs (Díaz et al., 2021, Mardones et al., 2021) as well as other oceanographic processes (Pérez-Santos et al., 2021, Soto-Riquelme et al. 2023). It has also been utilized for studying sub-domains within this Patagonian region (Pinilla et al., 2020; Díaz et al., 2021).

The time frame for the modeling process extended over six years, from 2016 to 2021. The use of two overlapping domains, specifically D1 Chiloe and D2 Aysen was influenced by computational capacity, resulting in a staggered development over time, from 2016 onwards. Initially, the D1 Chiloe domain was developed, followed by the D2 Aysen domain. The model configuration for both domains assumes a hydrostatic variant of the MIKE 3 model, with vertical discretization executed via hybrid coordinates: surface-based sigma coordinates and z-level coordinates in the bottom layers. The model included 55 layers for D1 Chiloe and 40 layers for D2 Aysen, which were utilized to accurately depict stratification, focusing on the highest resolution in the upper water column (approximating ~ 1m near the surface). Horizontal eddy viscosity was characterized using the Smagorinsky model (Smagorinsky, 1963), while the vertical viscosity was incorporated through the $\kappa - \epsilon$ turbulence scheme, which solves the transport equations for both turbulent kinetic energy (κ) and turbulent dissipation rate (ϵ) (Rodi, 1984). Bathymetry was based on SHOA nautical chart soundings (horizontal resolution of 500 meters), and a digital elevation model was constructed using the natural neighbor method (Sibson, 1981). This domain was discretized using triangular elements of different sizes. The highest resolution was observed in coastal, narrow, and shallow areas, with an average element size of ~300 m, whereas the spatial resolution near the boundary was ~1000 m.

Atmospheric forcings, such as wind stress and heat fluxes over the sea surface, were introduced using spatially and temporally varying fields from the WRF-IFOP atmospheric model (Skamarock et al., 2008). The WRF model, with its superior spatial resolution of 3 km compared to global models, enables a more accurate representation of the complex fjord topography. The performance of the WRF model was evaluated as described by

Pinilla et al. (2020). Soto-Riquelme et al. (2023) evaluated the performance of the WRF-IFOP model near the Guafo Mouth and confirmed the its effective correlation with meteorological stations in at area. Notably, their results revealed a high correlation with atmospheric pressure ($R=0.99$), accompanied by significant correlations for wind direction: $R=0.81$ for the east-west component and a more robust correlation of $R=0.94$ for the north-south component (Soto-Riquelme et al., 2023).

Freshwater sources were identified through the FLOW-IFOP hydrological model, which employs precipitation and temperature series data from the CR2MET gridded product (<http://www.cr2.cl/datos-productos-grillados/>). Using this data, characterized by a spatial resolution of 5×5 km, enables the simulation of runoff and the calculation of daily discharge series. Based on FLOW-IFOP estimates, the average annual freshwater discharge entering the D1 Chiloé domain during the 2016–2021 period was approximately $2545 \text{ m}^3 \text{ s}^{-1}$, while for the D2 Aysén domain, it was approximately $3126 \text{ m}^3 \text{ s}^{-1}$. The performance of the FLOW-IFOP model at the gauged river stations of the Chilean Water Authority can be accessed at <http://chonos.ifop.cl/flow/>. Furthermore, the correlations for the three main rivers in these regions—Puelo, Palena, and Aysén, Table S1, Fig. S1—were found to be 0.88, 0.76, and 0.87 respectively (see Fig. S2 in the supplementary material).

The water levels at the open boundary were set using harmonic analysis (Pawlowicz et al., 2002), based on a regional barotropic model data (Pinilla et al., 2012). The performance of water levels at seven locations (Table S1, Fig. S1) is presented as supplementary material (Table S2, Figure S3). The results demonstrate robust correlations between the sea level at different stations, with minimum correlations ranging from 0.93 to 0.97 (Table S2). Additionally, they exhibited an appropriate amplification of amplitude particularly in the northern area of this domain (Puerto Montt and Comau fjord) (Figure S3).

The flow data at the boundaries were set to zero in our hydrodynamics model, leading to internal balance in the current dynamics within the model domain across both spatial and temporal scales. The performance of the current data within the models contrasted with the ADCP data from different mooring points (Figure S1, Table S1), as shown in the supplementary material (Figures S4 and S5). The hydrodynamic model current was evaluated against the current velocities gathered by the ADCP. An empirical orthogonal function analysis (Thomson and Emery, 2014) was performed on the currents (both observed and modeled) to discern if the model could accurately depict the dominant modes of variability identified with the observations. Similar analyses have been previously performed to assess the suitability of hydrodynamic models in Patagonia (Pinilla et al., 2020, Soto-Riquelme et al., 2023).

Mode 1 plus Mode 2 accounted for over 95% of the variance in the model, whereas they accounted for approximately 86% of it in the observations, except in the Quitralco fjord, with a 77% variance observed in the model and 62% in the ADCP (Figure S4). The distribution of these percentages of variance between the model and the ADCP was correlated with an R-value of 0.96, as shown in Figure S5, which highlights the distinctiveness of the Quitralco fjord. On the other hand, the spatial vertical structures of Modes 1 and 2 between the model and the ADCP data were identical, generally showing agreement in barotropic structures, two-layer baroclinic structures, and even three-layer structures, as observed in the Quitralco fjord (Figure S4). Though the model is not without flaws, our

analysis suggests an agreement between the modes of variability, further implying a proficiency of the model in representing the processes vital to water transport in different locations.

365 The temperature and salinity boundary conditions were derived from CTD profiles obtained during CIMAR FIORDOS oceanographic cruises (Guzman and Silva 2002; Silva and Guerra 2004; Valdenegro and Silva 2003; Carrasco and Silva 2010). The performance of temperature time series and salinity fields within the model are presented as Supplementary Material. The model demonstrated commendable alignment in replicating the annual temperature cycle at various depths and locations (Table S1, Figure S1), generally exhibiting R-values above 0.78. An exception was observed in the Moraleda Channel at a depth of 120 m, where a lower R-value (0.28) was recorded (Figures S6 and S7).

370 To assess the water masses present within the fjords, salinity was employed as a key parameter. High salinity waters ($>33.5 \text{ g kg}^{-1}$), associated with SAAW and ESSW ocean masses, enter the deep layer of the Guafo mouth, traverse the Corcovado Gulf, and end their journey in the deep layers of the Puyuhuapi Fjord and Jacaf Channel. A reduction in salinity, indicative of Estuarine Water (EW), is also observed due to the melting of ice from the San Rafael Lagoon. The model's task was to accurately depict the arrival of specific salinity categories inside the fjords and channels (see Figure S8 in the Supplementary Material). Although the 34 g kg^{-1} isohaline is not visually present within the model domains, we believe the model successfully replicates the spatial structure, which suggests that the processes controlling salinity transport within the fjords were successfully incorporated. While the model may not perfectly replicate these processes, it does allow us to understand the fundamental physical transport mechanisms at play.

375 The MIKE 3 FM hydrodynamic model data were used to calculate the flushing time via a conservative tracer. According to Takeoka (1984) and Mosen et al. (2002), flushing time is defined as the time required for the total mass of a material within a specific area—such as a fjord, sound, or bay—to be reduced by a factor of e^{-1} (approximately 37%) (Prandle, 1984). The interior and exterior of the area were assigned initial concentration values of 1 and 0, respectively. Over the course of the simulation, the original water mass of the basin was incrementally replaced with inputs from open boundaries and rivers. This variable symbolizes the proportion of original water in each element within the area of interest at a given time, thereby, facilitating the identification of less flushed areas within the modeled basins (Andrejev et al., 2004). The final values were derived from a temporal average from 2016 to 2021, and a vertical average was calculated from 50 m to the bottom, which represents the area that typically displays the lowest oxygen values. In the present study, the flushing time was implemented in the Ecolab module of the MIKE 3 FM for every fjord within D1_Chiloé and D2_Aysén.

380 To gain a better understanding of the physical forcing related to the DO dynamics, we used the hydrodynamic model MIKE 3 FM (DHI, 2019), which solves continuity, momentum, temperature, and salinity transport equations. Specific features of MIKE 3 FM, such as equations, parameterizations, and their numerical schemes, are described in the DHI, 2019. In this study, two high-resolution model domains include the North Patagonian inner sea named D1_Chiloé ($41.3^\circ \text{ S} - 43.7^\circ \text{ S}$) and D2_Aysén, with an area from 43.6° S to 46.8° S (Figures 1d, 1e). Bathymetry was based on SHOA nautical chart soundings, and a digital elevation model was

400 constructed using the natural neighbor method (Sibson, 1981). This domain was discretized using triangular elements of different sizes. The highest resolution was observed in coastal, narrow, and shallow areas, with an average element size of 300 m, whereas the spatial resolution near the boundary was 1000 m.

The modeling period covered six years (2016–2021). The boundary conditions of temperature, salinity, currents, and sea level were based on CTD stations from different cruises conducted in the northern Patagonian fjords, most of which are included in Table 1. In addition, atmospheric forcings, such as wind stress and heat fluxes over the sea surface, were introduced using spatially and temporally varying fields from the WRF-IFOP (Weather Research and Forecasting Model of the Instituto Fomento Pesquero) atmospheric model. Finally, the performance of the WRF model was evaluated as described by Pinilla et al. (2020).

410 The freshwater sources were based on the FLOW-IFOP hydrological model, which uses precipitation and temperature series from the CR2MET gridded product (<http://www.cr2.cl/datos-productos-grillados/>) with a spatial resolution of 5 km × 5 km. Using this information, the runoff is simulated, and the daily discharge series is calculated. According to the information estimated by FLOW-IFOP, the average annual freshwater discharge entering domain D1_Chiloé was $\sim 2545 \text{ m}^3 \text{ s}^{-1}$, while in D2_Aysén it was $3126 \text{ m}^3 \text{ s}^{-1}$ for the period 2016–2021, this includes the main rivers but also all those larger than the annual mean $> 5 \text{ m}^3 \text{ s}^{-1}$ supplied by FLOW-IFOP. The performance of the FLOW-IFOP model at the gauged river stations of the Chilean Water Authority (www.dga.cl) is available at <http://chonos.ifop.cl/flow/>.

420 The MIKE 3 FM hydrodynamic model data was utilized in calculating the flushing time via a conservative tracer. According to Takeoka (1984) and Mønsen (2002), flushing time is defined as the time required for the total mass of a material within a specified area - such as a fjord, sound, bay, etc. - to be reduced by a factor of e^{-1} (approximately 37%) (Prandle, 1984). The interior and exterior of the area were assigned initial concentration values of 1 and 0 respectively. Over the course of the simulation, the original basin's water mass was incrementally replaced with inputs from open boundaries and rivers. This variable symbolizes the proportion of the original water in each element within the area of interest at a given time, thereby facilitating the identification of less flushed areas within the modeled basins (Andrejev et al., 2004). Furthermore, the final values are derived from a temporal average from 2016 to 2021 and a vertical average was calculated from 50m to the seabed - the zone typically displaying the lowest oxygen values. In the present study, the flushing time was implemented in the Ecolab module of the MIKE 3 FM for every fjord within D1_Chiloé and D2_Aysén.

430 Information from the hydrodynamic model MIKE 3 FM was used to calculate the flushing time by applying a conservative tracer. The flushing time, according to Takeoka (1984) and Mønsen (2002), was defined as the time necessary for the total mass of material within an area of interest (fjord, sound, bay, etc.) to be reduced by a factor of e^{-1} (~37%) (Prandle, 1984). The initial concentration values assigned were 1 for the inner side and zero for the outer side of the area. During the simulation, the water mass from the original basin was gradually replaced by inputs from open boundaries and rivers. This variable represents the amount of the original water in each element within the domain of interest at a given time. Therefore, it can be expected to identify the less flushed areas within the modeled basins (Andrejev et al., 2004).

In the present study, the flushing time was implemented in the Ecolab module of the MIKE 3 FM for every fjord within D1_Chiloé and D2_Aysén. We validated the spatial salinity pattern in the hydrodynamics model using salinity as a proxy for water mass categories; therefore, when comparing the model and observations (CTD station) along North Patagonia showed good agreement, higher salinity ($>33 \text{ kg}^{-1}$), associated with SAAW and ESSW ocean waters, enters the deep layer of the Guafo mouth, crosses the Corcovado Gulf, and ends its travel at the deep layers of the Puyuhuapi Fjord and Jacaf Channel. Furthermore, a decrease in salinity due to ice melting from the San Rafael Lagoon is also seen, which indicates the presence of estuarine water (EW) (See Figure S1).

3 Results

3.1. Long-term annual mean of hydrographic-chemical parameters

The long-term annual means include all data sets presented in Figures 2a and 2b. This section scrutinizes the behavior of conservative temperature, absolute salinity, DO, and inorganic nutrients. The long-term seasonal mean of conservative temperature (CT) denoted warmer water in the northern region (41.5° – 43° S) during both seasons, between the Desertores Pass and the Reloncaví Fjord (Figure 2c-d). In contrast, cold waters were observed in the deep layer of the Puyuhuapi Fjord and Jacaf Channel, but colder water was registered in San Rafael Lagoon. This location also had the lowest absolute salinity ($S_A=15$ – 21 gkg^{-1}), indicating the presence of estuarine water (EW) owing to the contribution of the ice melting from the San Rafael Lagoon and rivers discharges (Figure 2a2e-bf). In this area, the EW moved from south to north and mixed with the Subantarctic oceanic water (SAAW), contributing to the origin of the Modified Subantarctic oceanic water (MSAAW), as was observed in the vertical-horizontal salinity distribution. Moreover, EW was also observed in the northern domain of the study area, especially at the surface layer in the Reloncaví system and the Comau and Reñihue fjords, contributing to the formation of the MSAAW. In this region, the origin of EW was mainly attributed to the freshwater supply from river discharge. We identified two different sources favoring the presence of EW and formation of the MSAAW: 1) The combination of ice melting from the San Rafael Lagoon with river discharge in the southern region and 2) the freshwater supply by river discharge in the northern region. Both sources contributed to the difference in conservative temperature observed in the MSAAW.

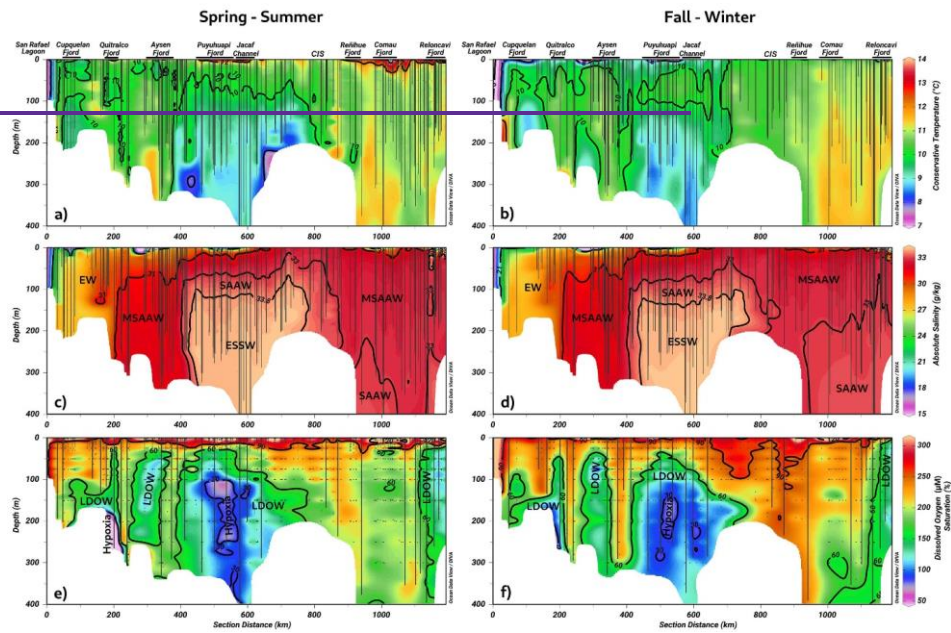
The EW was also observed at the surface layer in the Reloncaví system all year round, but SAAW was presented especially during the fall-winter season. Finally, the Equatorial Subsurface water (ESSW) enters the deep layer of the Guafo mouth, crosses the Corcovado Gulf, and ends its travel at the deep layers of the Puyuhuapi Fjord and Jacaf Channel. During the fall-winter season, a slight reduction in ESSW distribution was observed (Figure 2e2e-2df).

In the area contained by the ESSW, low DO (LDOW) and hypoxic waters were observed, but. Again, LDOW was registered at Reloncaví Fjord, where but this time they were not related to the ESSW was not observed.

In general, the Chiloé Inner Sea showed aThe main seasonality difference highlighted the homogenization of the water column, mainly observed during the fall-winter seasons, in which high DO values (267 – $312 \mu\text{mol L}^{-1}$) and oversaturated waters ($< 100\%$ DO Saturation) were registered in the Chiloé Inner Sea

(CIS). Additionally, more extensions of the hypoxic conditions and LDOW were registered during the spring-summer seasons (Figure 2e2g–2fh). Apparent oxygen utilization showed higher values ($\sim 200 \mu\text{mol kg}^{-1}$) in areas where LDOW and hypoxia were detected (Figure 2i-j).

Table 4 details the statistical characteristics of the water masses identified in this study. Furthermore, Figure 3 shows a TS diagram representing the quantification of water masses, which highlights the dominance of the MSAAW, with 60.96% and 54.67% proportions during the spring-summer and fall-winter seasons, respectively. The SAAW was the second dominant water mass, with 15.25% and 22.64% proportions, followed by the EW. Finally, the ESSW showed the smallest proportion, with 10.77% and 11.15% values. The ESSW was generally characterized by cold, salty, and poor DO water when compared to those of the EW, MSAAW, and SAAW (Table 4 and Figure 3).



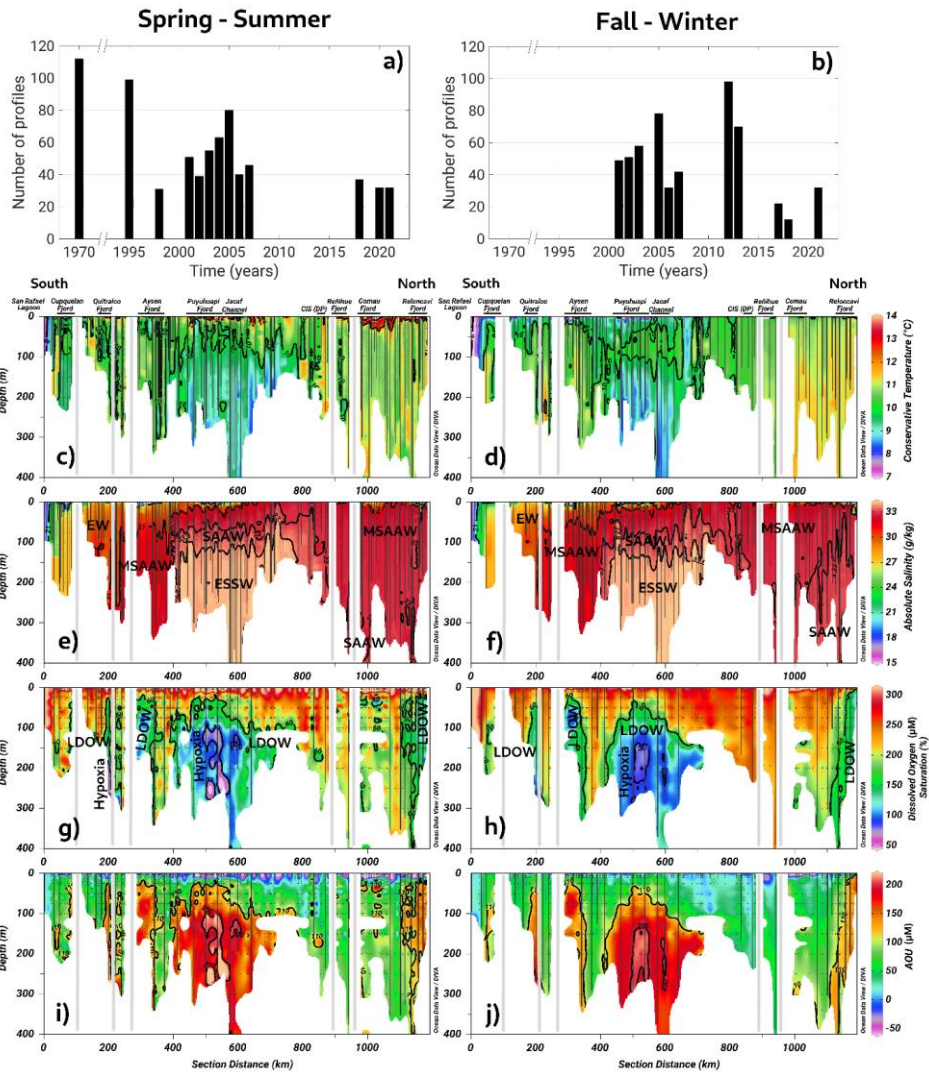


Figure 2. (a, b) Time series of CTD profiles used to compute seasonal averages. Long-term seasonal means of (a-b) conservative temperature, (c-d) absolute salinity, and (e-f) dissolved oxygen hydrographic (a-d) and chemical (e-f) parameters collected along a vertical section in the northern Patagonian fjord during the fall-winter and spring-summer seasons.

490

Table 4. Statistical characteristics of the water masses identified in the northern Patagonian fjords.

Salinity criteria (Sievers and Silva, 2008)		Spring-Summer Campaigns				Fall-Winter Campaigns			
Water masses	Salinity range (g kg ⁻¹)	Water masses (%)	CT Mean Std ^a	S _A (g kg ⁻¹) Mean Std	DO (μmol L ⁻¹) Mean-Std	Water masses (%)	CT Mean Std	S _A (g kg ⁻¹) Mean Std	DO (μmol L ⁻¹) Mean-Std
EW	0–31	12.64	10.29 ±1.1	27.92 ±4.7	245.25 ±65.8	11.92	9.70 ±0.8	28.75 ±3.4	238.02 ±56.8
MSAAW	31–33	60.96	10.64 ±0.5	32.44 ±0.5	197.11 ±46.2	54.67	10.55 ±0.6	32.34 ±0.5	231.82 ±37.6
SAAW	33–33.8	15.25	10.49 ±0.6	33.25 ±0.2	196.03 ±41.9	22.64	10.85 ±0.6	33.19 ±0.2	208.34 ±46.1
ESSW	33.8>	11.15	9.12 ±0.4	34.11 ±0.1	109.57 ±32.6	10.77	9.27 ±0.5	34.13 ±0.1	114.77 ±36.0

^aStd: standard deviation.

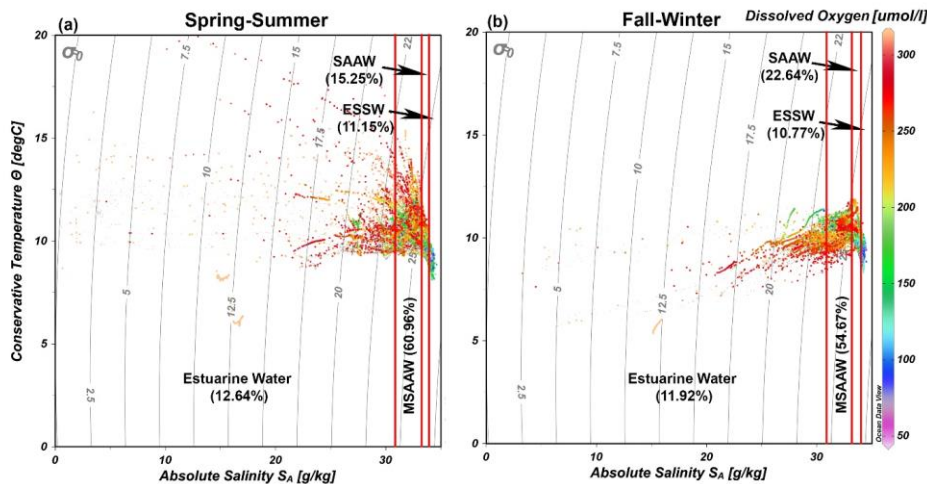
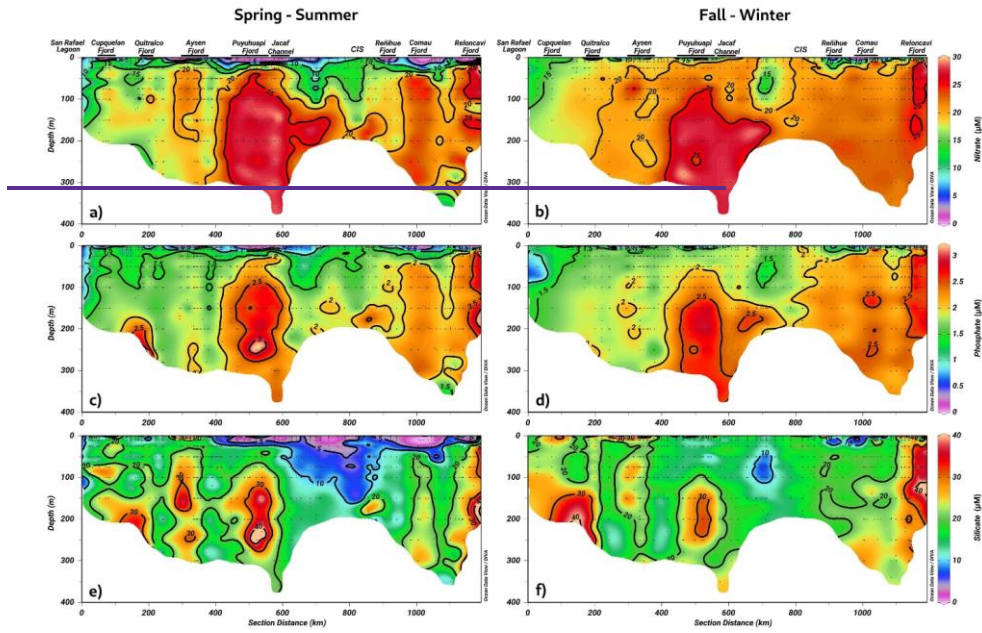


Figure 3. Temperature/salinity (TS) diagram with dissolved oxygen records showing the representation of water masses identified during (a) spring-summer and (b) fall-winter seasons in the northern Patagonian fjords. The dataset utilized in the TS diagram is described in Table 1.

As previously shown, the Puyuhuapi Fjord and Jacaf Channel were regions where high-salinity and hypoxic-LDOW waters were registered. In addition, a high concentration of inorganic nutrients was observed in the subsurface layer at a depth of 50 m (Figure 34). In the Puyuhuapi Fjord and the Jacaf Channel, between 100–300 m depth, nitrate (Figure 3a4a), phosphate (Figure 3e4c), and silicic acid (Figure 3e4e) range from 25–30 μM, 2–3 μM, and 30–50 μM, respectively. A second area with high inorganic nutrients was detected in the Reloncaví system, in which the highest absolute values of surface silicic acid were registered during the fall-winter season (e.g., 210 μM). Comparing seasonal concentrations, the fall-winter season showed the highest abundance in the water column.

However, the absolute maximum nitrate (Figure 3b4b), phosphate (Figure 3d4d), and silicic acid (Figure 3f4f) values were recorded in the subsurface layer during the spring and summer seasons.



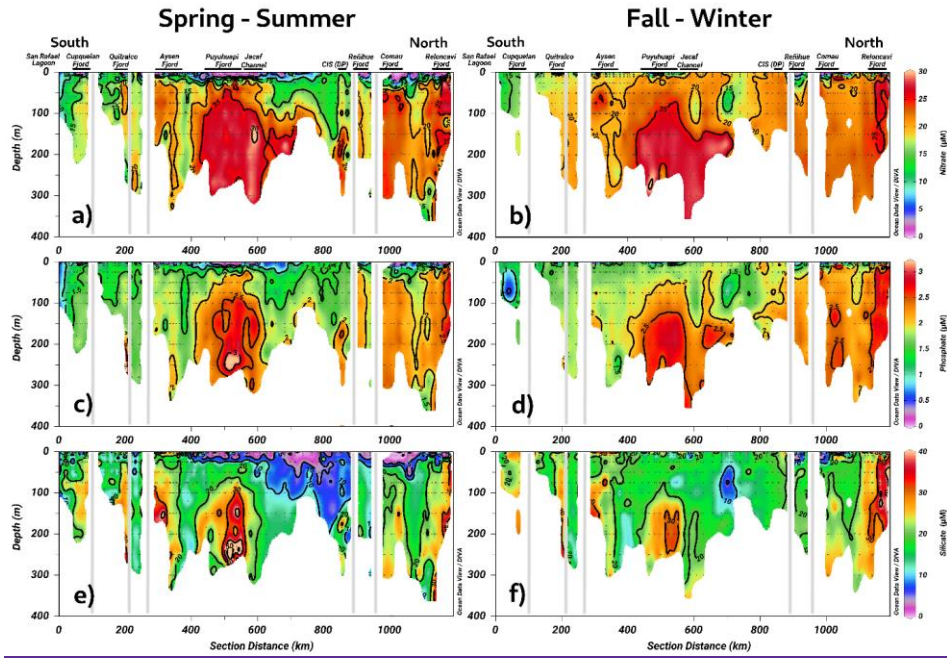
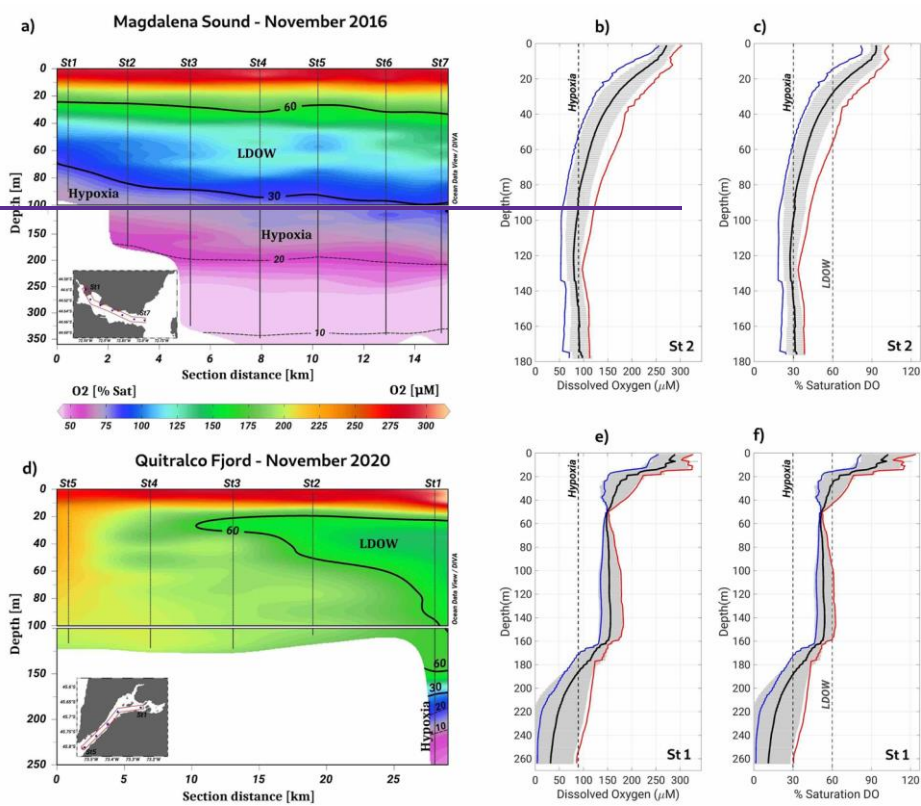


Figure 34. Long-term seasonal mean of inorganic nutrients. (a, b) Nitrate, (c, d) phosphate, and (e-f) silicate collected along a vertical section in the northern Patagonian fjord system during fall-winter and spring-summer seasons.

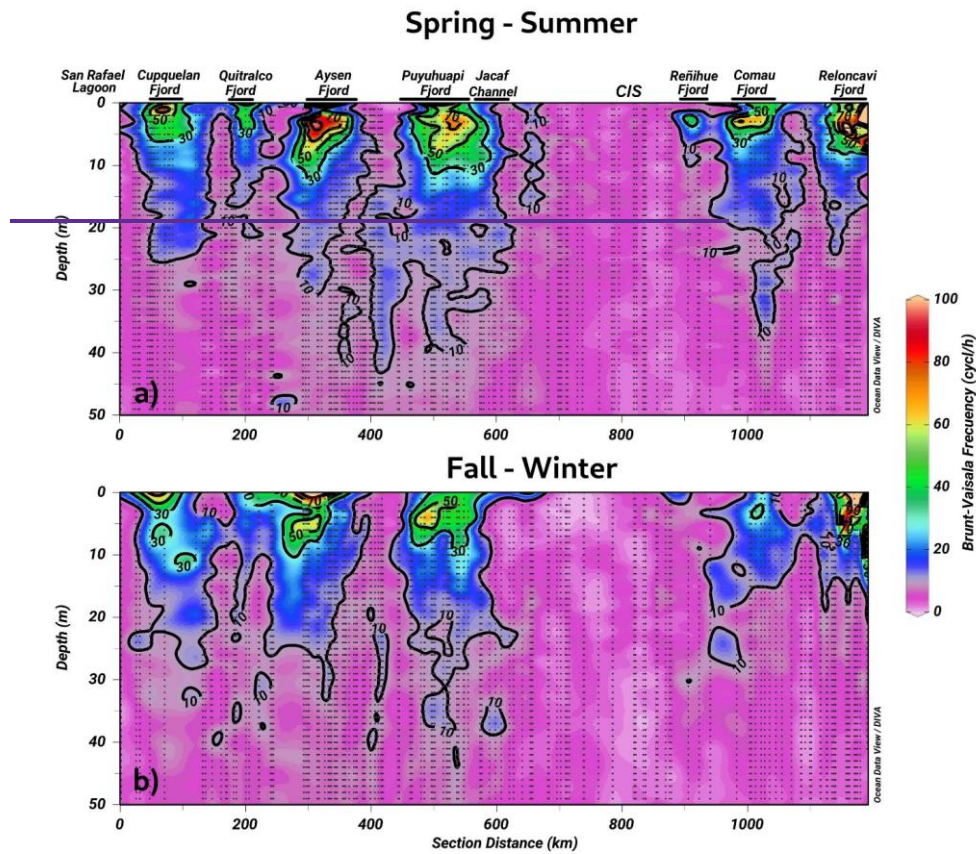
515 The analysis of hypoxia and LDOW conditions in the northern Patagonian fjord system highlighted the presence of two areas with water bodies with these characteristics, e.g., the Puyuhuapi Jacaf and the Reloncaví regions. Moreover, Magdalena Sound (44.6° S / 72.9° W) showed shallower hypoxia over the entire Patagonian region. At this location, a 30% DO saturation isoline was observed at a depth of 70 m, and the LDOW reached a depth of approximately 20 m (Figure 4a-c). On another side, the lowest DO values of the northern Patagonian fjord system, specifically 9.36 $\mu\text{mol L}^{-1}$ and 1.6% oxygen saturation, were recorded at the deepest layer (~200 m) of the Quitralco Fjord (45.7° S / 73.3° W) (Figure 4d-f).

520



525 **Figure 4.** Vertical section of dissolved oxygen carried out along (a, b) Magdalena Sound (44.65° S / 72.87° W) and (c, d) Quitralco Fjord during November 2016 and November 2020, respectively. In (b, c, e, f), red, black, and blue lines represent absolute maximum, average, and minimum values of the DO, respectively. The grey horizontal lines show the standard deviations calculated using 16 profiles for Magdalena Sound and 3 profiles for the Quitralco Fjord.

530 The calculation of the Brunt-Väisälä frequency (BVF), a parameter-variable used to identify
mixed/stratified regions, evidenced a permanent mixing of the water column in the Chiloé inner sea ($BVF \leq 10$ cycl
 h^{-1}) (Figure 5a-b). Furthermore, the homogenization of physical (e.g., conservative temperature and absolute
salinity) and chemical (e.g., DO oxygen and inorganic nutrients) variables was observed in these regions. On
another side, stratified water (between 2 and 10 m depth) was detected during spring-summer inside the fjords, e.g.,
Cupquelan, Quitalco, Aysén, Puyuhuapi, Comau, and Reloncaví, showing values over $BVF \geq 50$ cycl h^{-1} (Figure
535 Figure 5a).



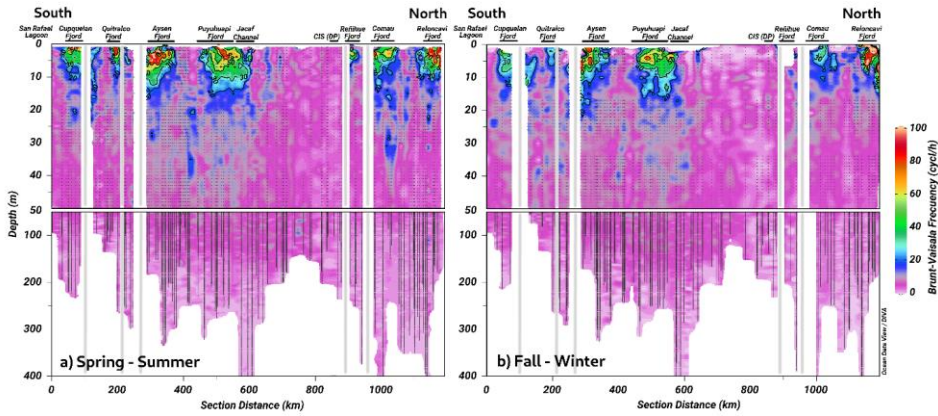
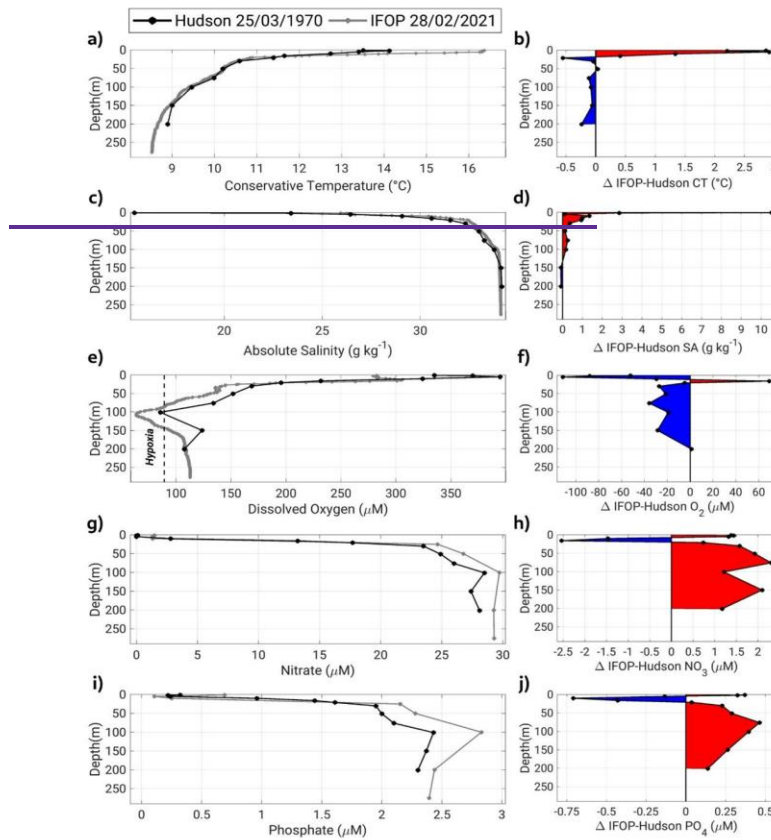


Figure 5. The long-term seasonal mean of Brut-Väisälä frequency along a vertical section in the northern Patagonian fjord during the (a) spring-summer, and (b) fall-winter seasons.

545

A comparison between oceanographic conditions measured in a similar station in Puyuhuapi Fjord (Figure 6), but 50 years apart, denoted deoxygenation of approximately $30\text{--}40\ \mu\text{mol L}^{-1}$ registered from 50–150 m depth (Figure 6e–f). At the same layer, the conservative temperature decreased ($\sim 0.2\ ^\circ\text{C}$) (Figure 6a–b). Furthermore, the absolute salinity (Figure 6c–d) and inorganic nutrients, specifically, nitrate ($\sim 2\ \mu\text{mol L}^{-1}$) and phosphate ($\sim 0.5\ \mu\text{mol L}^{-1}$) increased (Figure 6g–j). A rate of increase of nutrient concentration by year can be estimated, in the case of nitrate, to be $0.04\ \mu\text{mol L}^{-1}\text{year}^{-1}$, and for phosphate, $0.01\ \mu\text{mol L}^{-1}\text{year}^{-1}$.



550

Figure 6. (a, c, e, g, i) Comparison of hydrographic and chemical profiles in a station located in Puyuhuapi Fjord ($44.7^\circ\text{ S}/72.8^\circ\text{ W}$) during the Hudson (March 25, 1970) and IFOP (February 28, 2021) oceanographic cruises. (b, d, f, h, j) show the difference between profiles.

3.3. DO and chlorophyll-a features from sporadic oceanographic cruises

The analysis of hypoxia and LDOW conditions in the northern Patagonian fjord system highlighted the presence of two areas with water bodies with these characteristics: the Puyuhuapi-Jacaf and Reloncaví regions. Moreover, Magdalena Sound (44.6° S, 72.9° W), located between the Puyuhuapi Fjord and the Jacaf Channel (Figure 1), showed the shallowest hypoxia over the entire northern Patagonian fjords. At this location, a 30% DO saturation isoline was observed at a depth of 70 m, with the LDOW reaching a depth of approximately 20 m (Figure 6a–c). Additionally, the lowest DO values of the northern Patagonian fjord system (9.36 $\mu\text{mol L}^{-1}$ and 1.6% oxygen saturation) were recorded at the deepest layer (~200 m) of the Quitalco Fjord (45.7° S, 73.3° W) (Figure 6d–f).

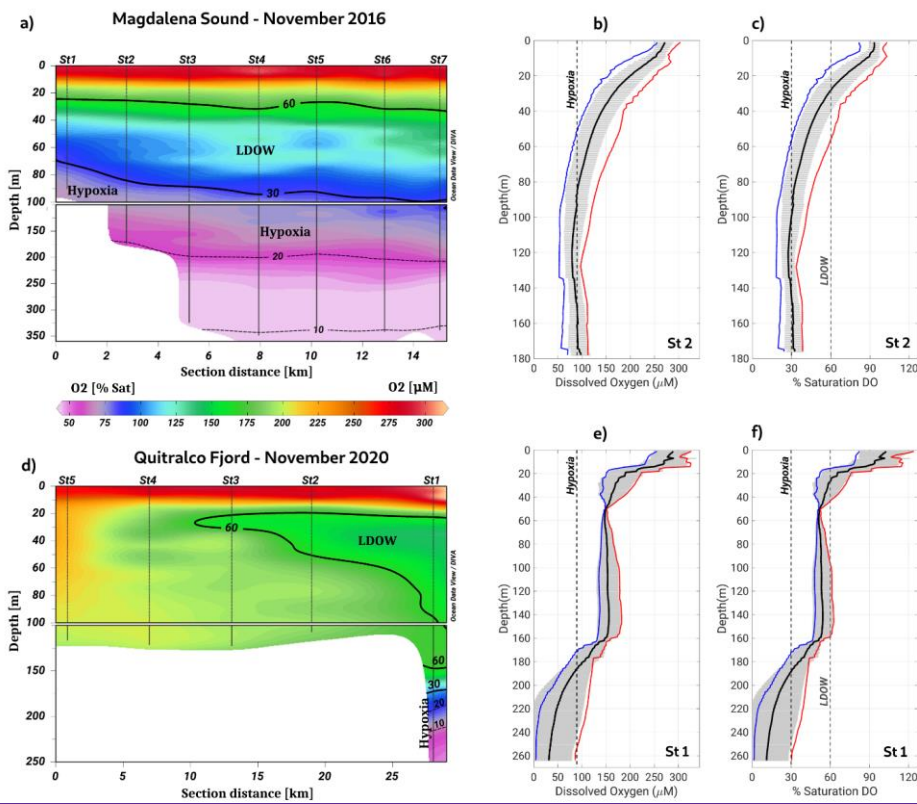
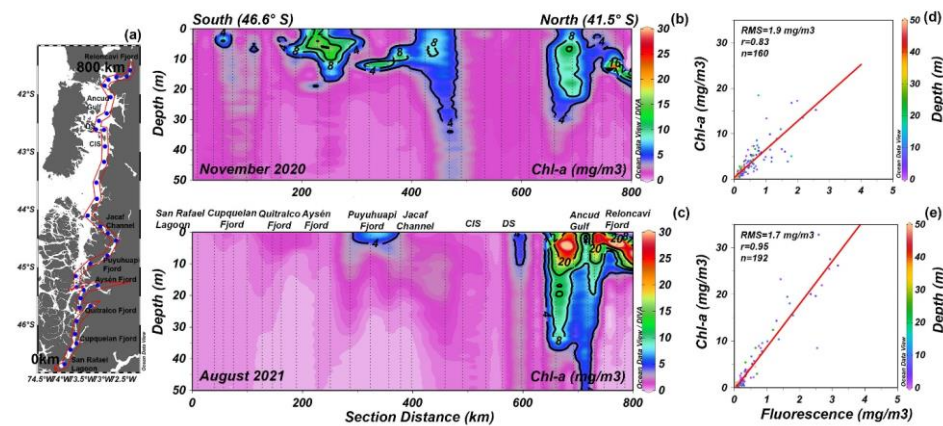


Figure 6. Vertical section of dissolved oxygen along (a-c) Magdalena Sound and (d-f) Quitalco Fjord during November 2016 and November 2020, respectively. In (b, c, e, f), red, black, and blue lines represent the absolute maximum, average, and minimum values of DO, respectively. Grey horizontal lines show the standard deviations calculated using 16 profiles for Magdalena Sound and 3 profiles for the Quitalco Fjord.

The chlorophyll-a (Chl-a) data collected during two oceanographic campaigns (Figure 7a) denoted high concentrations of Chl-a in the Reloncaví Fjord, the Puyuhuapi Fjord, and the Jacaf Channel (Figure 7b, 7c) where LDOW and hypoxia conditions were registered. The Chl-a values observed during the winter season in the Reloncaví Fjord were exceptionally high (32.8 mg m^{-3}). This observation is scrutinized in the discussion section. Regardless, in general, the winter season of August 2021 showed a deficiency of Chl-a in the southern part of the study area (Figure 7c). The vertical distribution of the Chl-a data described before was obtained through a statistical analysis between the fluorescence data from CTD (every 1-m depth) and the in-situ Chl-a samples from discrete levels (i.e., 0, 5, 10, 15, 25, and 50 m) (Figure 7d, 7e).

570



575

Figure 7. Distribution map of the stations. Vertical distribution of chlorophyll-a (Chl-a) obtained during (b) November 2020 and (c) August 2021 in the northern Patagonian fjords. (d and e) Statistical relationship between the fluorescence data from CTD and in-situ Chl-a samples. In (d and e) RMS is the root mean square and n is the number of data points used to obtain the R-values.

580

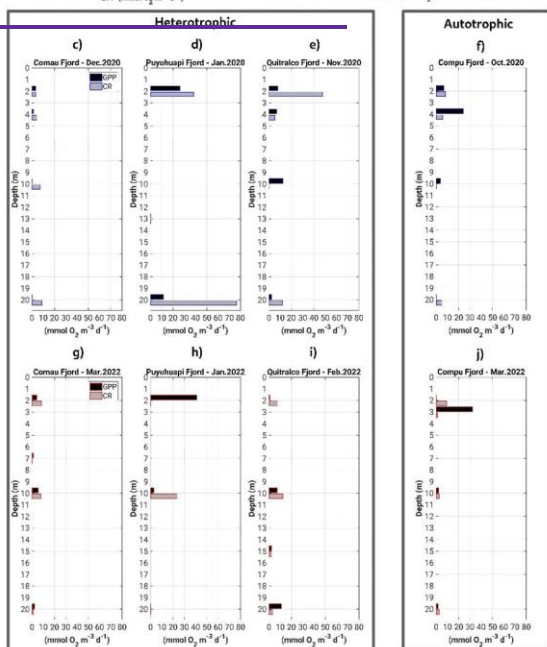
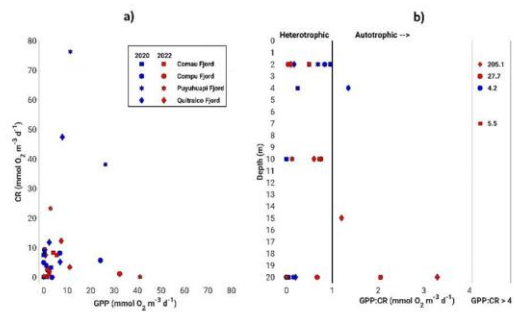
3.2. Rates of primary production, community respiration, and bacterial production

The GPP and CR estimates obtained in our sampling campaigns agreed well with the measurements reported in previous studies for the Patagonian fjords during the productive period (Iriarte et al., 2007; Montero et al., 2011; Montero et al., 2017a). The GPP and CR rates showed a weak coupling was observed between the GPP and CR rates, with most experiments indicating that less oxygen is produced than consumed (Figure 7a8a). Thus, most fjords exhibited heterotrophic metabolism ($GPP:CR < 1$) in the surface layer (0–20 m) during the study period (Figure 7b8b). The highest rates of GPP in terms of oxygen (18.6 to $41.02 \text{ mmol O}_2 \text{ m}^{-3} \text{ d}^{-1}$) were mainly recorded in the upper 5 m of the water column, whereas the lowest values (0 to $17.6 \text{ mmol O}_2 \text{ m}^{-3} \text{ d}^{-1}$) were observed between 10 and 20 m depth (Figure 7e8c, 7j8j). CR rates did not show a definite vertical pattern, registering highest (23.3 to $76.3 \text{ mmol O}_2 \text{ m}^{-3} \text{ d}^{-1}$) and lowest (0 to $12.3 \text{ mmol O}_2 \text{ m}^{-3} \text{ d}^{-1}$) values throughout the water column (0–20 m) (Figure 7e8c, 7j8j).

590

Throughout the study period in different fjords, integrated GPP and CR rates (down to 20 m) ranged from 0.1–2.6 g C m⁻² d⁻¹ and from 0.8–6.6 g C m⁻² d⁻¹, respectively, (Figure 89, Table 2). Neither rate showed significant differences ($p > 0.05$) between spring-summer 2020–2021 (Figure 8a9a) and summer of 2022 (Figure 8b9b).
595 Although there were no significant differences ($p > 0.05$) between GPP values recorded from different fjords in both study periods (Figure 8a9a, 8b9b), Comau Fjord showed the lowest rates of GPP (0.1 to 0.6 g C m⁻² d⁻¹) whereas Puyuhuapi and Reloncaví fjords showed the highest values (1.9 to 2.6 g C m⁻² d⁻¹). In the case of CR, the highest rates were recorded in Puyuhuapi Fjord (2.2 to 6.6 g C m⁻² d⁻¹) and the lowest in Comau Fjord (0.8 to 0.9 g C m⁻² d⁻¹) (Figure 8a9a, 8b9b). The phytoplankton composition in the study area showed a similar pattern to the GPP values, highlighting maximum abundances on the surface and minimal abundances at a depth of 20 m (data not shown). In addition, Comau Fjord showed the lowest abundances (66×10^3 cell L⁻¹) whereas Reloncaví Fjord showed the highest concentrations of phytoplankton ($1,227 \times 10^3$ cell L⁻¹).
600

Estimated rates of BSP ranged between 0.05 and 0.6 g C m⁻² d⁻¹ within the study area and were positively and significantly correlated with GPP values (Figure 89, Table 2). The percentage of GPP utilized by bacteria ranged from 3% to 56%, except in Comau Fjord, where a higher utilization percentage (151%) was recorded, suggesting that more organic carbon is consumed than is produced locally.
605



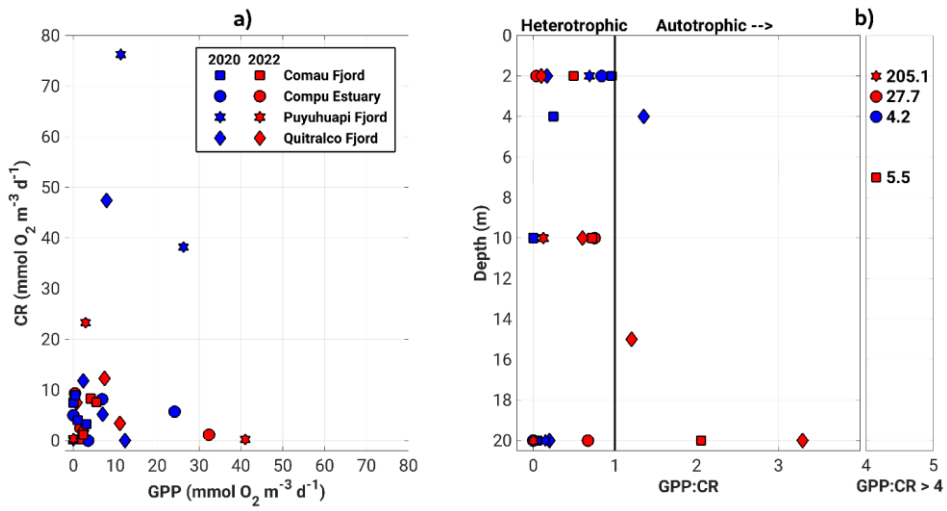


Figure 78. (a) Relationship and (b) vertical patterns of all datasets from the GPP and CR. (c–j) represents the vertical distribution of GPP and CR obtained during experiments of primary production on (c–f) spring-summer of 2020–2021, and (g–j) summer of 2022. GPP: Global primary production, and CR: community respiration.

610

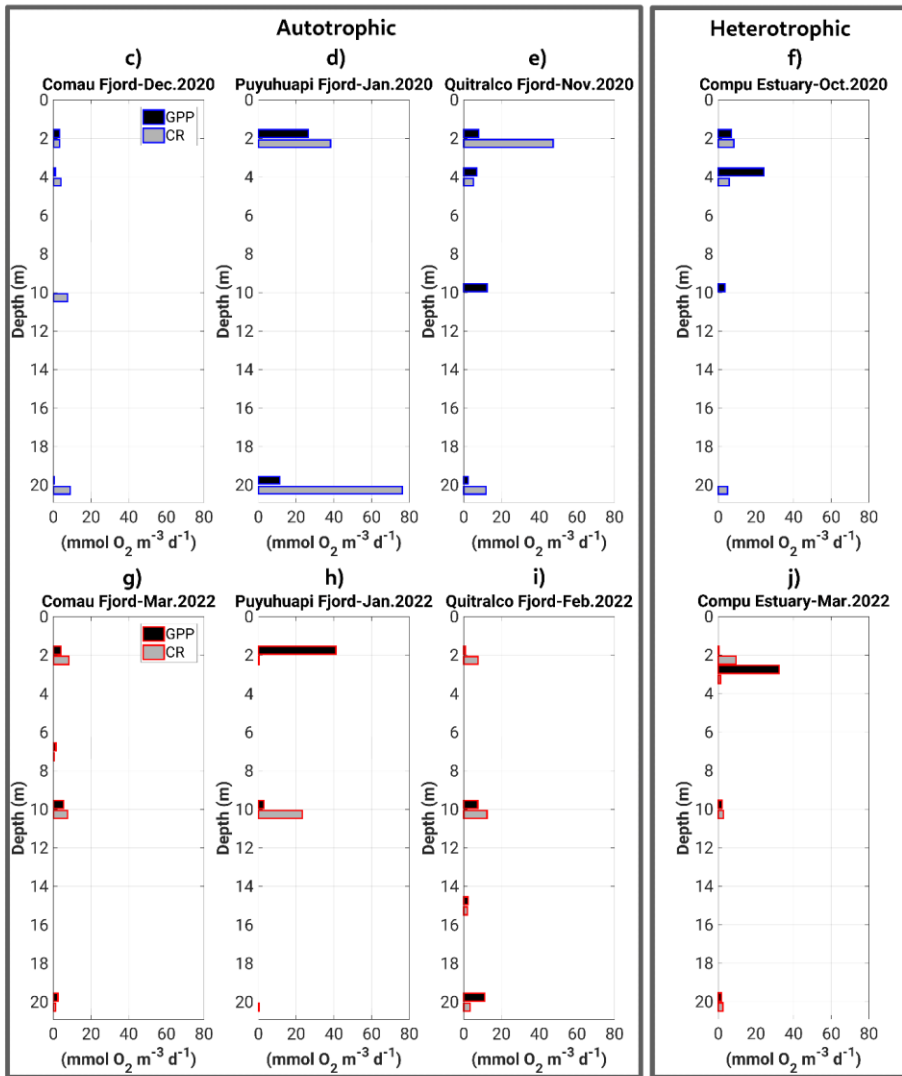
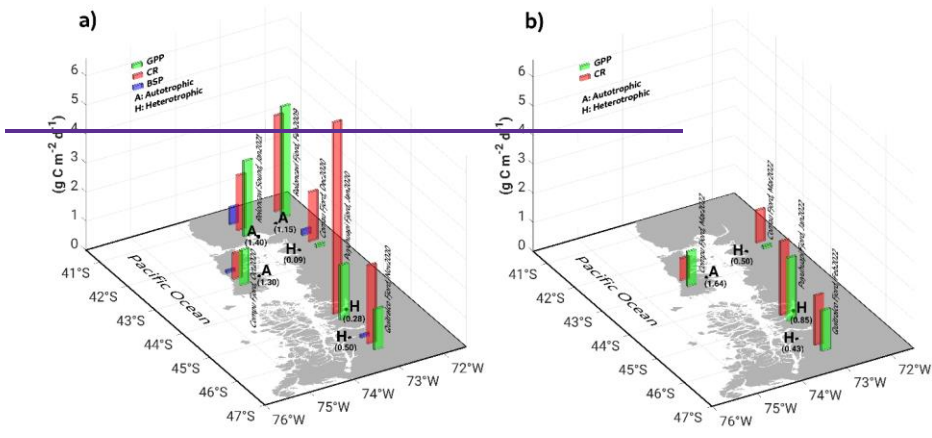


Figure 8. Continued.



620

Figure 89. In-situ experiment of primary production during (a) spring-summer of 2020–2021, and (b) summer of 2022, covering some fjords in the northern Patagonian fjord system. GPP: Global primary production, CR: Community respiration, BSP: Bacterial secondary production. Results shown from Reloncaví Fjord in (a) were extracted from Montero et al., (2011).

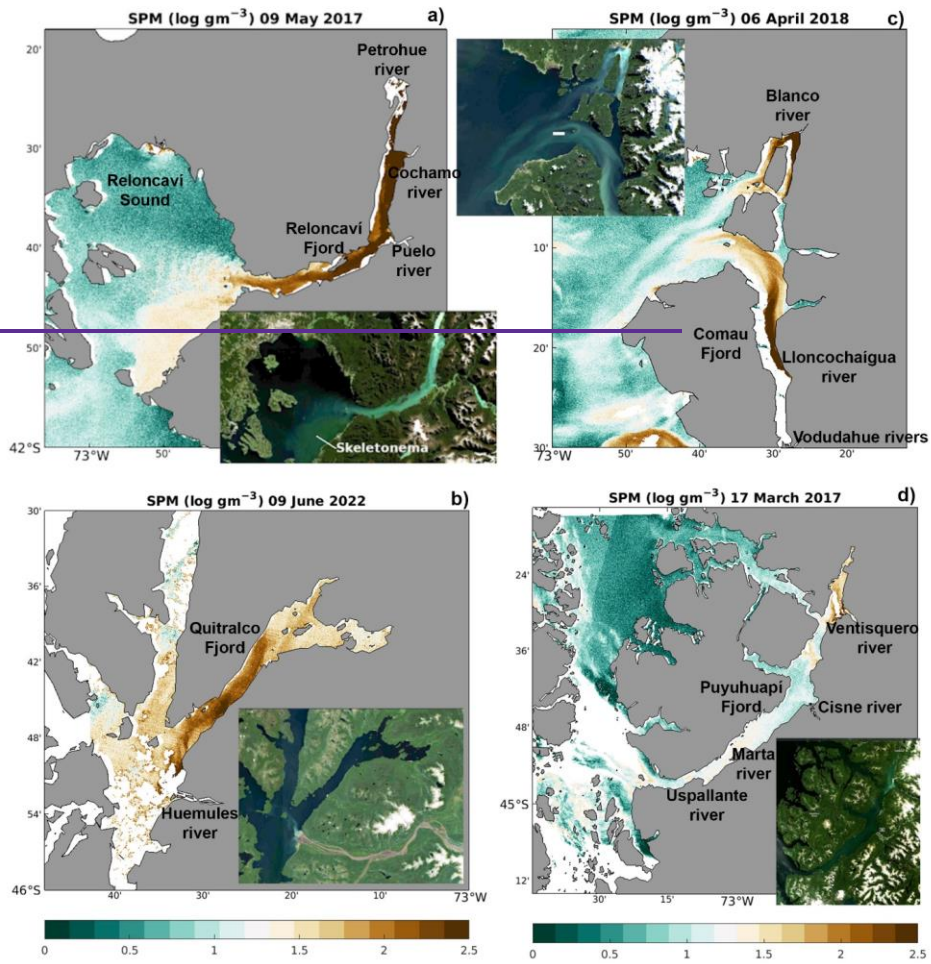
625

3.3. Satellite image of organic matter supply to fjords

Satellite images show that freshwater inputs into the sea were accompanied by large amounts of suspended sediments (Figure 910), possibly acting as a source of allochthonous organic matter, favoring the heterotrophic metabolism reported in the previous section. On May 9, 2017, a large amount of suspended matter flowed into the

630 Reloncaví Sound from its fjord, mainly dominated by three rivers: Petrohue, Cochamo, and Puelo (Figure 9a10b). In
the southeast part of the Reloncaví Sound, the observed high concentration of sediments was due to the presence of
a diatom bloom (evidenced by greenish waters in the southeast part of the Reloncaví Sound), mainly formed by
Skeletonema costatum, which attained concentrations of more than 5 million cells L⁻¹ within the fjord (Figure not
shown). This bloom affected both the eastern part of the Reloncaví Sound and the Reloncaví Fjord. While the
635 amount of suspended matter visible in the Sentinel-2 images was generally homogeneously high along the fjords
e.g., on June 9, 2022, in the Quitralco Fjord (Figure 9b10c), and May 9, 2017, in Reloncaví, (Figure 9a10b). Some
examples of this phenomenon, such as the one on April 6, 2018, on Comau Fjord (Figure 9d~~e~~), show a very
heterogeneous distribution of suspended sediments within the fjord, suggesting the influence of the currents in the
distribution of waters rich in sediment. On this date, waters flowing from the river Blanco in the northern part of the
640 fjord's mouth were whitish in color, indicating carbonate-rich sediments. Water flowing into this fjord from the
south, principally from the Lloncochaigua and Vodudahue rivers, has a more brownish color, indicating a higher
quantity of organic matter.

At the Quitralco Fjord (Figure 9b10c), suspended sediments from Rio de los Huemules (at 73.30° E 45.54° S, the
brown riverbed is clearly visible in the natural color insert) appeared to propagate within the fjord, affecting the
645 water clarity along the entire fjord. Inspection on other dates (not shown) revealed high variability in the direction of
the river outflow, sometimes entering the fjord (and staying there for extended periods), and sometimes being
directed towards the south. Finally, the Puyuhuapi Fjord also registered a high signal from suspended sediments due
to river discharge; for example, the Vestiquero River was located at the fjord head (Figure 9d10e). Other rivers, such
as the Cisnes, Marta, and Uspallante, could also influence the supply of allochthonous organic matter to the
650 Puyuhuapi Fjord, contributing to a decrease in DO and hypoxia. However, the cloud cover does not allow for better
satellite images.



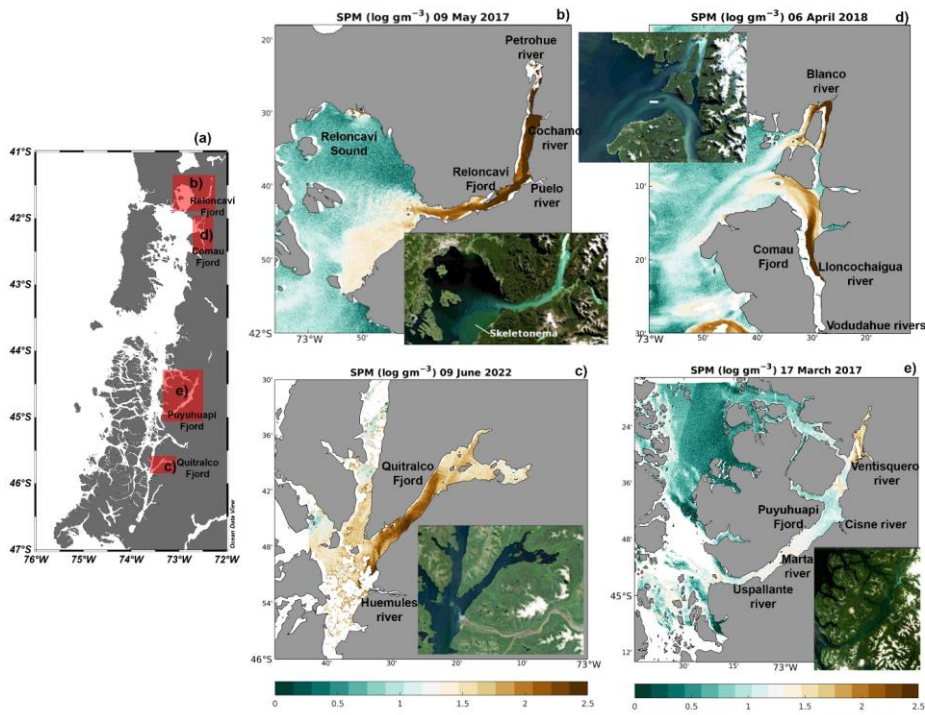


Figure 9. (a) Map showing the study sites. Suspended particulate matter as measured by Sentinel 2 on (ab) Reloncaví Sound, (bc) Quitalco Fjord, (cd) Comau Fjord, and (de) Puyuhuapi Fjord.

660 3.4. Biogeochemical variables parameters

665 We observed differential signals of SPM (Figure 11b) along a latitudinal transect conducted from north to south in the northern Patagonia fjords (Figure 11a). Specifically, significant increases in SPM were registered at the surface layer of the mouths of the Comau and Aysén fjords. Furthermore, in the southern region, the SPM levels were high at the subsurface layer (50–150 m) from San Rafael Lagoon to Jacaf Channel, with maximum values exceeding 4 mg L⁻¹, except in Quitalco Fjord, which showed values close to 2 mg L⁻¹. Similar conditions were observed in the transition zone between the Puyuhuapi Fjord and Jacaf Channel. In the central region, within the Chiloé Inner Sea, SPM values were minimal. In the northern area, a small subsurface core near Comau Fjord and the Reloncaví system exhibited an increase in SPM. Along the water column, characteristic cores were found in the inner channels south of the study area, between 45° S and 47° S. Other deep but less intense cores (<3 mg L⁻¹) were located in the Inner Sea of Chiloé and Reloncaví system.

670 The percentage of allochthonous organic carbon (%POC_{allo}) exhibited an irregular distribution in the southern area, with surface minimums under 30% at the mouths of the Quitalco, Aysén, and Puyuhuapi fjords

(Figure 11c). In the northern area, the Comau Fjord and Reloncaví Sound presented low %POC_{allo} values. Along the water column, %POC_{allo} appeared to increase with depth, reaching values of approximately 70%, except in the Inner Sea of Chiloé, where it was under 50%. The C:N ratio showed more homogeneous values at the surface layer (C:N<8) (Figure 11d) but increased from a 50-m depth until the seabed (C:N>12), especially in the region between the San Rafael Lagoon and the Jacaf Channel, coinciding with the high SPM region presented in Figure 11b. In the Chiloé Inner Sea, the C:N ratio decreased along the water column.

The isotopic signal of the carbon ($\delta^{13}\text{C}$) increased in the same sites where %POC_{allo} decreased, with values ranging from -25‰ to -15‰ (Figure 11e). At the subsurface layer, $\delta^{13}\text{C}$ signal became lighter than that in the surface. An exception was observed in the Chiloé Inner Sea and the transition zone between the Aysén Fjord and San Rafael Lagoon, where the C:N ratio coincidentally decreased. In the region extending from the southern Chiloé Inner Sea to Aysén Fjord, elevated levels of isotopic signal of nitrogen ($\delta^{15}\text{N}$) enrichment were observed, primarily at the surface and subsurface levels (Figure 11f). Notably, there was a significant increase in nitrogen values, with some exceeding 9%; particularly, in the Chiloé Inner Sea, the enrichment extended to depths of 150–200 m.

Notable observations were made regarding the concentrations of CDOM in the Patagonian fjords region, with high concentrations throughout the water columns in the north area, spanning from the Chiloé Inner Sea to the Reloncaví system (Figure 11g). Conversely, in the southern area, CDOM concentrations declined, with minimum values as low as 20 $\mu\text{g L}^{-1}$ of specific UV absorbance between the Jacaf Channel and San Rafael Lagoon. Despite this overall decrease, localized increases in CDOM concentrations were identified in certain fjords, such as Aysén, Quitraco, and the San Rafael Lagoon. These subsurface concentration spikes highlight the spatial variability of CDOM distribution within the fjord system. Moreover, these findings provide valuable insights into the spatial distribution patterns of CDOM in the Patagonian fjords, indicating higher concentrations in the northern region and a decline towards the southern end of the study area. The localized increases in CDOM concentrations in specific fjords suggest the influence of local processes or inputs contributing to the observed spatial heterogeneity.

South of the study area (Figure 10a), the suspended particulate matter (SPM) (Figure 10b) was high from Puyuhuapi Fjord to San Rafael Lagoon, with maximum values $> 4 \text{ mg L}^{-1}$. In the north area, a little sub-surface core close to Comau Fjord and the Reloncaví system showed an increase in the SPM. The % of POM allochthonous (POM_{allo}) showed an irregular distribution (Figure 10c), with a subsurface minimum $< 30\%$ in the mouth of Quitraco, Aysén, and Puyuhuapi fjords in the south and, Comau and Reloncaví system in the north. The POM_{allo} increased with depth, reaching approximately 70%, except for the Chiloé Inner Sea, where POM_{allo} was less than 50%. The C:N ratio shows sub-surface values < 8 at depths above 50 m (Figure 10d), and increasing values to depth greater than 15 m from Jacaf Channel to the San Rafael Lagoon. In the Chiloé Inner Sea, the autochthonous organic matter increased. The isotopic signal showed an increase in the same sites where the % POM_{allo} decreased, with values between -25‰ and -15‰. At depth, the organic matter showed light relative to the surface (Figure 10e). High nitrogen enrichment values were evident at the surface level from the south of Chiloé Inner Sea to the Aysén Fjord (Figure 10f), showing a significant increase with values $> 9\%$ up to 150 m in the Chiloé Inner Sea. High concentrations of CDOM were observed north of the Patagonian fjords (Figure 10g) along all water columns. To the

Comentado [A1]: Please specify in which direction. From the surface to the seabed?

Comentado [A2]: This is defined as "isotopic composition of the sample" in the previous text. Please choose a single way to refer to this term and use it consistently.

south of the study system, there was a decrease in CDOM concentration with minimum values as low as $20 \mu\text{g L}^{-1}$ SQU, from Jacaf Channel to San Rafael Lagoon.

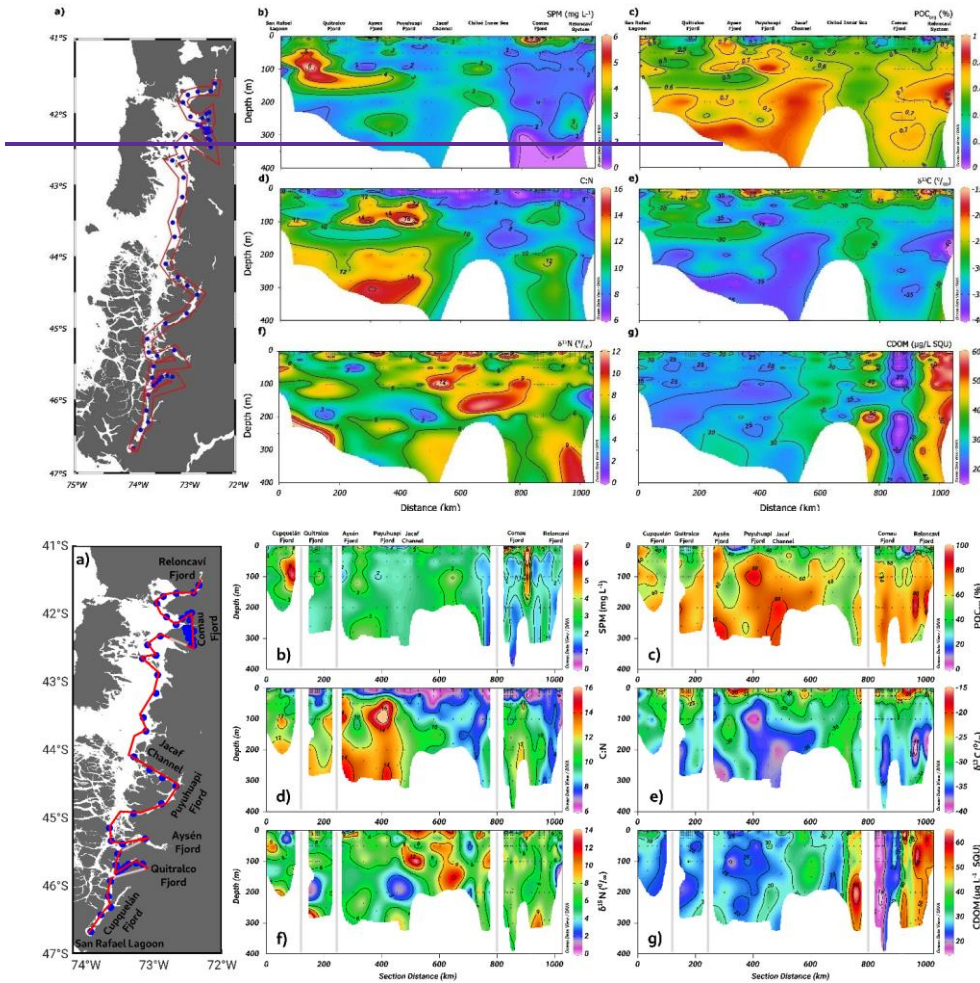
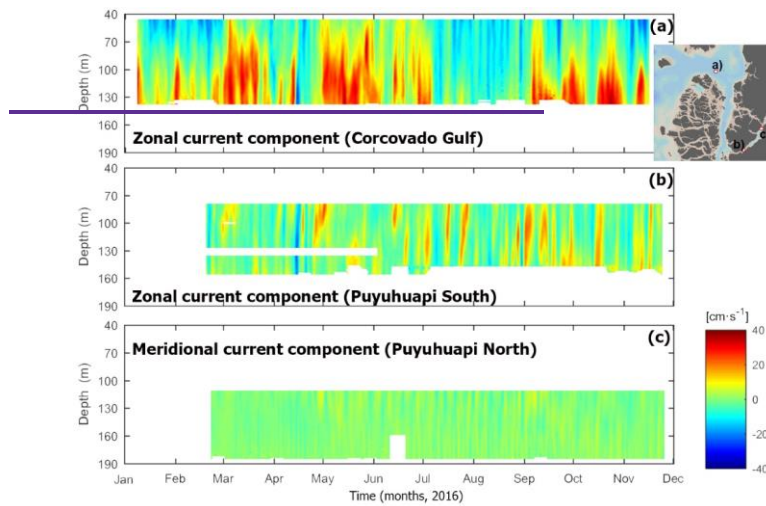


Figure 10 Figure 11. (a) Study area showing transect (red color) used to biogeochemical study case carried out in November 2020 during Expeditions PN-I IFOP. (b) Suspended particular material (SPM), (c) allochthonous carbon percentage (POC_{allo}), (d) Carbon and nitrogen ratio (C:N), Isotopic signal of (e) δ¹³C and (f) δ¹⁵N, and (g) Chromophoric Dissolved Organic Matter (CDOM).

720 3.5. Circulation regime from ADCP measurements

The low-frequency deep circulation (> 40 m depth) in the inner sea of the region showed a marked east-west regional gradient in the along-channel current amplitude (Figure 11Figure 12). The Corcovado currents were dominated by an eastward flow with a maximum intensity of approximately 30 cm s⁻¹ (Figure 11Figure 12a-b), whereas at the mouth of the Puyuhuapi Fjord (Figure 11Figure 12c-db), the maximum current was approximately 10 cm s⁻¹.

725



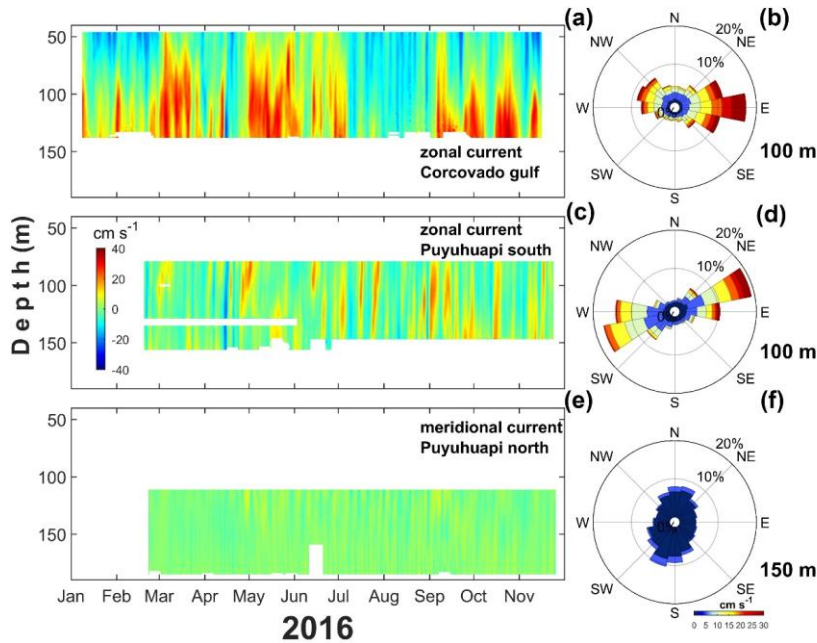


Figure 12. Subtidal deep circulation regimens obtained with ADCP performed in the (a) Corcovado Gulf and in (b,c, e) southern-northern zone of the Puyuhuapi Fjord from January to November 2016. (b, d, and f) Marine current rose obtained at 100 m (Corcovado Gulf), 100 m (Puyuhuapi south), and 150 m (Puyuhuapi north) depths.

The Corcovado currents showed a marked pattern in the 40–70 m layer, which was dominated by westward currents, and short-duration events of approximately 20 cm s^{-1} were observed throughout the entire time series. This strong westward flow seems to be associated with the austral spring-summer seasons (January–March and November–December 2016); however, a weak ($\sim 5 \text{ cm s}^{-1}$) and longer (July–October 2016) westward flow was observed during the austral winter-autumn period. In the layer between 70 and 130 m, eastward (and strong) currents dominated, and there were periods of one to two months with eastward flow during March–April, May–July, and September–December 2016 with currents $> 20 \text{ cm s}^{-1}$. The layer between 100 and 130 m showed maximum currents of approximately 40 cm s^{-1} at the end of October 2016 (Figure 12a).

Puyuhuapi Fjord currents were obtained at the southern mouth (South Puyuhuapi, Figure 12c-d) and middle fjord (North Puyuhuapi, Figure 12e-f). At the mouth of the fjord, low-frequency currents showed short pulses that covered most of the 70–160 m layer; typically, those pulses were eastward without an evident seasonal pattern. A unique low-frequency westward event was observed in mid-April 2016, which was also present in the Corcovado Gulf. In general, the currents in southern Puyuhuapi were weak ($< 10 \text{ cm s}^{-1}$); however, during September and October 2016, eastward events of 20 cm s^{-1} were observed. In northern Puyuhuapi, most currents

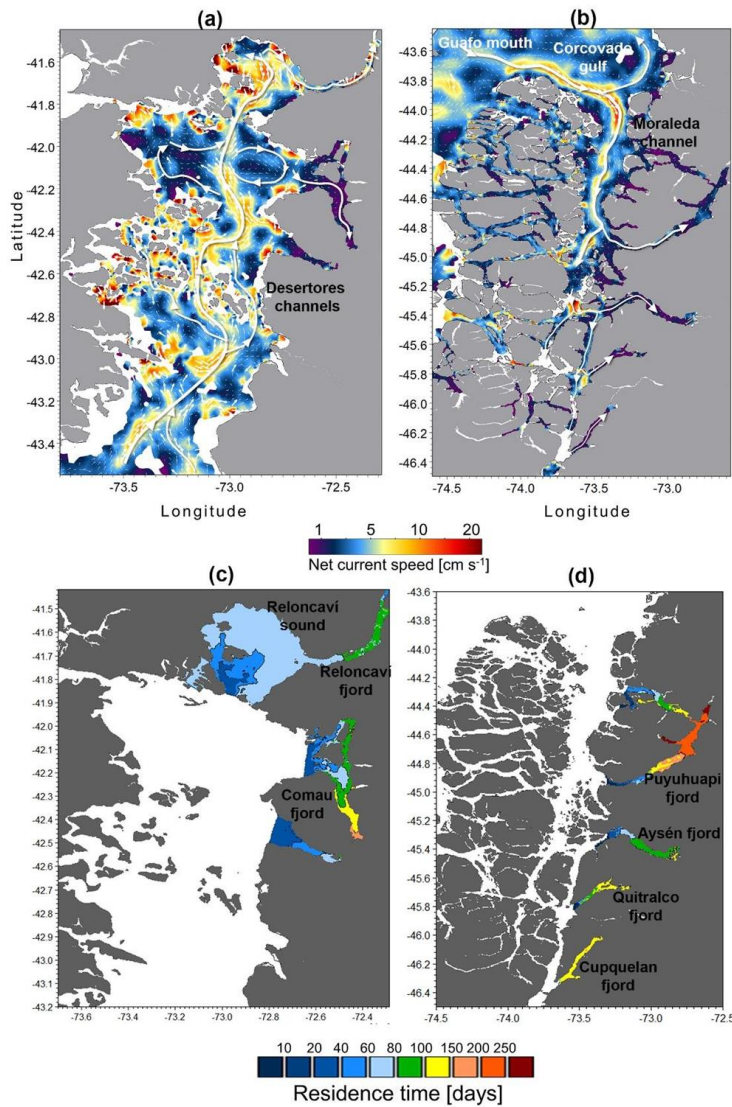
were weak ($< 10 \text{ cm s}^{-1}$) without a temporally or spatially evident pattern, and the flow tended to be northward and intensified between May and September 2016.

750

3.6 Circulation regimen oceanographic model

Deep currents, defined as subtidal or residual currents (average of 50–300 m) over the three years of simulation, have a relatively large spatial variation (Figure 13a, 13b). Consequently, the model could correlate the most energetic zones in the outer channels with those of lower energy inside the fjords. ~~This result becomes clearer when looking at Figures 12a and 12b, which show the spatial variability of the net current speed.~~ In general, the exchanges between the fjords and ocean registered high average velocities, that is, the Guafo mouth, Moraleda Channel, Corcovado Gulf, and Desertoires PassChannel, with net current velocities ranging from 10 to 20 cm s⁻¹. In contrast, in the fjords, the average velocity of the deep ~~current-flow~~ was less than 5 cm s⁻¹. The predominant flow was generally towards the interior of the fjords (Figure 13a, 13b).

755



760 **Figure 12** **Figure 13.** (a, b) Map showing the deep currents regime in northern Patagonian fjords. The deep current
 was defined as subtidal currents calculated as the average of currents from 50–300 m depth. (c, d) The residence
 time was calculated for each fjord of the northern Patagonian. (a-d) Data were obtained from the hydrodynamic
 model MIKE 3 FM developed by IFOP.

The flushing/residence time calculated for each fjord showed that the sector towards the head of Puyuhuapi Fjord registered the longest retention time (>200 days). In comparison, the shortest times were found in the Reloncaví Sound-Fjord (60–90 days), except for the Reloncaví Fjord head, which reached values close to 100 days (Figure 42e-13c and 42d-13d). Comau Fjord showed relatively high values, which increased from north to south. In the central part of Comau Fjord, the residence time ranged from 90 to 120 days, whereas at the fjord head, it ranged from 150 to 190 days. Meanwhile, the Aysén Fjord showed residence time values lower than 120 days, which were higher towards the fjord head, whereas the Quintralco Fjord reported 150 days at the fjord head and 100 days at its central part. Finally, the Cupuelán Fjord exhibited greater homogeneity throughout the fjord, with relatively high values ranging from 120 to 150 days. Most studies reported a spatial gradient of water retention, with the highest values found near the fjord's head.

4. Discussion

Oceanographic research in the Patagonian fjords started in 1995 with CIMAR-fjords project, supported by the Chilean Navy. As an oceanographic sampling strategy, Patagonia was divided into three zones, e.g., northern (41°–47° S), central (47°–53° S), and southern (53°–55.8° S) Patagonia, and the frequency of the cruises were primarily seasonal (Sievers, 2008). Moreover, some oceanographic cruises, such as the Hudson expedition in 1970, occurred in this zone (Table 1). The data collected through the CIMAR projects allowed us to understand the main physical (water mass quantification) and chemical (e.g., dissolved oxygen and inorganic nutrients) processes impacting this fjord system, such as the hypoxic conditions due to the influence of the ESSW (Sievers, 2008; Sievers and Silva, 2008; Silva, 2008; Silva and Vargas, 2014; Schneider et al., 2014; Pérez-Santos et al., 2014). Furthermore, some studies about biological processes that include the consumption of DO, such as respiration and the remineralization of organic matter, other studies have also contributed to the understanding of the processes that favoring hypoxia and the reduction of DO depletion, such as primary production and community respiration, associated with the abundance of different phytoplankton species (Montero et al., 2011; 2017; Iriarte et al., 2018). Additionally, the development of hydrodynamic models helped to determine the areas where the water age was significantly high, for example, the Puyuhuapi Fjord (Pinilla et al., 2020), and where stronger mixing stratification occurred (Ruiz et al., 2021). Recently, satellite data from suspended sediments have allowed us to understand the supply of allochthonous organic matter to fjords due to river discharge. Therefore, t. This study scrutinized all processes contributing to the presence of water under hypoxic conditions and LDOW in the northern Patagonian fjords, as discussed in the next section.

4.1 Water masses proprieties and biogeochemical processes in northern Patagonian Fjords

Recent and historical hydrographic data collected from the Patagonian fjords, especially in the northern area, confirmed the presence of analogous water masses detected previously by the Hudson oceanographic cruise in 1970. EW, MSAAW, SAAW, and ESSW were recorded from the surface layer to the bottom (to a depth of approximately 500 m) (Figure 3-2 and Figure 63). Similar patterns were recognized in terms of the vertical-horizontal distributions, highlighting the location of the salty-hypoxic-LDOW and nutrient-rich waters associated

with the ESSW in the Jacaf Channel and Puyuhuapi Fjord (Figure 2 and 4). This water mass enters Patagonia by the Guafo mouth and moves south throughout the Moraleda Channel to end at the Puyuhuapi Fjord and Jacaf Channel (Linford et al., 2023). On the other hand, the EW dominated in the southern area due to freshwater input from the San Rafael Lagoon and rivers discharge, which is characterized by oxygenated waters due to its high solubility. Finally, SAAW and MSAAW covered the entire study area (Figure 2), as reported by Siever and Silva (2008), Schneider et al., (2014), Pérez-Santos et al., (2014), and Pinilla et al., (2020).

The absence of stratification ~~Vigorous vertical mixing~~ was observed throughout the year in the Chiloé Inner Sea (Figure 5). In this area, ~~both~~ the physical and biogeochemical ~~parameters-variables~~ showed homogeneous values from the surface layer to the bottom (Figure 2 and Figure 34), indicating the presence of MSAAW (originating from mixing the SAAW with the EW). Furthermore, the calculation of the buoyancy frequency and potential energy anomalies using the output from the oceanographic model demonstrated that more robust mixing occurred in the Chiloé Inner Sea (Ruiz et al., 2021). This explains the importance of this area for DO ~~production-ventilation~~ and redistribution in the northern Patagonian fjords.

Water masses in northern Patagonia have unique physicochemical properties (Sievers and Silva, 2008; Silva, 2008; Silva and Vargas, 2014; Schneider et al., 2014; Pérez-Santos et al., 2014). ~~From a biogeochemical standpoint, there are no classifications of water masses in the Patagonian fjords, even though the biotic and abiotic processes that occur in every body of water respond to the biogeochemical cycles to some extent.~~ In the case of northern Patagonian fjords, EW is rich in silicic acid because of the riverine supply (Silva and Vargas, 2014), with characteristic pulses at the surface layer that changes throughout the year due to the organisms' consumption (Montero et al., 2011), as observed in northern Patagonia, including the Chiloé Inner Sea (Figure 34).

~~The SAAW is strongly connected with the estuarine water masses (MSAAW and EW), and the ESSW interacts with it, as shown in this study (Figures 2 and 3). Organic matter degradation processes occurred inside the fjords, mainly in terms of nitrogenous compounds being remineralized. These processes increase the nutrient pool that is originally transported by oceanic water and are responsible for the high accumulation of nitrate and phosphate registered in the subsurface layer of the Puyuhuapi Fjord and Jacaf Channel (Figure 4).~~

~~Inside the fjords, where low salinity from high river discharge dominated, a persistent halocline/pycnocline/stratified water column developed; therefore, deep-water ventilation by vertical mixing and diffusion with the oxic surface layer was limited (Figures 2–5). These conditions favored the occurrence of LDOW zones in the fjords, where stratification and particulate organic matter input were higher than at the mouths (Figure 10). Thus, DO consumption was favored owing to organic matter degradation in the Reloncaví, Comau, Puyuhuapi, Aysén, and Quintralco fjords (Figure 2), as was reported for the Milford Sound in New Zealand (Stanton, 1984), Framvaren Fjord in Norway (Yao and Millero, 1995), Lower St. Lawrence Estuary in Canada (Lefort, 2012), and Rivers Inlet in British Columbia (Jackson et al., 2022).~~

~~Similarly, organic matter production in the subsurface layers generates regions of high carbon concentration with an enriched isotopic signal of mainly autochthonous origin (Figure 10). Silva and Vargas (2014) reported an LDOW zone developed near the fjord heads ($<178 \mu\text{mol L}^{-1}$) because of more significant allochthonous particulate organic matter inputs transported by local rivers (Figure 9). However, there was a mixture~~

840 of organic materials, which is why the POM isotopic values were relatively lighter than those expected if the organic
matter pool was autochthonous. In any case, the enhanced organic matter input (autochthonous or allochthonous) to
the deep layer increased DO consumption owing to respiration and overwhelmed the oxygen supplied by horizontal
advection.

845 A latitudinal transect from north to south in the study area revealed distinct signals of SPM within the
fjords (Figure 11b). Although SPM concentrations generally fell within expected ranges, there was significant
variability, with values ranging from 0.5 to 500 mg L⁻¹ (Muñoz et al., 2014; Pryer et al., 2020). A noteworthy pattern
of increased SPM levels below the surface was observed at the fjord mouths, particularly in the southern part of the
study area. This finding suggests that fjord outlets play a crucial role in particulate organic matter accumulation,
850 potentially that originating from terrestrial sources. Furthermore, the high SPM values observed in the southern
region indicate substantial contributions of allochthonous material, which may be influenced by factors such as river
discharge, sediment resuspension, and glacial activity (Gonzalez et al., 2010). A more detailed analysis of SPM
distribution revealed irregular patterns in the percentage of allochthonous organic matter (%POC_{allo}). At the mouths
of the Quitalco, Aysén, and Puyuhuapi fjords, a subsurface minimum indicated relatively low terrestrial organic
855 matter inputs (Gonzalez et al., 2010). The low-level input of organic matter could be attributed to limited river
contributions or the autochthonous organic material production rate coinciding with nutrient depletion and increased
DO (Holding et al., 2017). In contrast, areas such as the Jacaf Channel and the Chiloé Inner Sea exhibited higher
contributions of %POC_{allo}, indicating a more significant influence of allochthonous sources. Further, the increase in
%POC_{allo} with depth highlights the importance of vertical transport and sedimentation processes in determining the
860 distribution of organic matter throughout the water column (Figure 11c). Considering that carbon fluxes and the
functioning of the fjord system are highly variable depending on the season of the year (Gonzalez et al., 2010), these
could potentially affect both the trophic webs and carbon export, which are more independent of local primary
production than coastal areas.

The C:N ratio exhibited spatial variability, with more homogeneous values in subsurface layers shallower
than 50 m (Figure 11d). On average, the bulk particulate organic carbon and nitrogen concentrations maintained a
865 C:N ratio of 8.5:1, exceeding the Redfield ratio of 6.6:1 typically observed in phytoplankton biomass within the
marine realm (Redfield, 1958). Notably, the southern region exhibited higher C:N ratios, coinciding with areas with
elevated SPM levels and increased %POC_{allo}. While these higher C:N ratios may be intuitively attributed to
terrestrial sources with a higher carbon content relative to nitrogen, a more plausible explanation may be the
increasing trend of the C:N ratio with depth. The observed C:N ratios suggest the influence of microbial
870 rem mineralization processes and the preferential removal of nitrogen-rich organic matter (Taucher et al., 2020). The
increase of the C:N ratio with depth likely reflects the consumption and degradation of sinking particles by
zooplankton and heterotrophic bacteria, resulting in the preferential remineralization of nitrogen (Figure 3) over
carbon and the subsequent elevation of the C:N ratio in sinking particles (Tomas et al., 1999; Schneider et al., 2003).

875 The spatial gradients of $\delta^{13}\text{C}$ have been previously documented in estuarine and continental shelf waters in
Patagonian fjords (Silva and Vargas, 2014; Gonzalez et al., 2010; Iriarte et al., 2018), but there is no evidence of
gradient of nitrogen isotopic signals prior to this study. Nevertheless, the pronounced phytoplankton bloom resulted

880 in an enrichment of $\delta^{13}\text{C}$ in SPM (Figure 11), similar to observations made in other fjords around the world (Remeikaite-Nikiene et al., 2017). The seasonal distribution of Chl-a evidenced the phytoplankton activity along the northern Patagonian fjords, especially during spring, 2020 (Figure 7). However, in winter of 2021, a phytoplankton bloom was registered in the Reloncaví Fjord and Ancud Gulf. Pérez-Santos et al. (2021) reported the occurrence of high Chl-a and an increase of phytoplankton in the Reloncaví Sound during late winters (August and September, 2017–2020) due changes in the water column conditions; e.g., stratification started when salinity decreased owing to the increase of river discharge mainly caused by ice melting. The stabilization of the water column is one of the main factors triggering primary production in the Patagonian fjords (Pérez-Santos et al., 2021). The isotopic carbon signals revealed an increase in $\delta^{13}\text{C}$ values where $\% \text{POC}_{\text{allo}}$ decreased, indicating a shift towards a more depleted isotopic signature. This suggests the predominance of marine-derived organic carbon in areas with lower inputs of allochthonous material (Kumar et al., 2016). Moreover, the lighter carbon isotopic signals observed with depth suggest isotopic fractionation processes associated with remineralization and the preferential utilization of more labile organic carbon by heterotrophic bacteria (Muñoz et al., 2014; Kuliński et al., 2014).

890 The spatial gradients of $\delta^{13}\text{C}$ have been previously documented in estuarine and continental shelf waters in Patagonian fjords (Silva and Vargas, 2008; Gonzalez et al., 2010; Iriarte et al., 2018), but there is no evidence of gradient of nitrogen isotopic signals. Nevertheless, the pronounced phytoplankton bloom resulted in an enrichment of $\delta^{13}\text{C}$ in SPM (Figure 10), similar to observations made in other fjords around the world (Remeikaite-Nikiene et al., 2017). In the same way, the enrichment of $\delta^{15}\text{N}$ of SPM results in primary production evidence that, in at least some regions of the fjords, the isotopic signals it was of mainly autochthonous origin (Figure 10). We did not establish a clear spatial gradient of $\delta^{13}\text{C}$ and $\delta^{15}\text{N}$ values in the Patagonian fjords. The results strongly indicate that the cause of the variability in C and N isotope fractionation was biological processes as previously demonstrated by Savoye et al., (2003) where the co-variation of $\delta^{13}\text{C}$ and $\delta^{15}\text{N}$ with seasonally changing abiotic factors, like temperature and nutrient concentrations, establishes the seasonal nature of $\delta^{13}\text{C}$ and $\delta^{15}\text{N}$ values as observed by reflecting the seasonal succession of phytoplankton species.

900 Elevated levels of nitrogen enrichment were primarily observed in the surface layer of the region extending from the southern Chiloé Inner Sea to the Aysén Fjord, indicating the influence of nitrogen inputs from sources such as river discharge, atmospheric deposition, and biological activity (Velinsky and Fogel, 1999). The significant increase in nitrogen values, particularly in the Chiloé Inner Sea, suggests the presence of enhanced nitrogen cycling and retention processes within this fjord system. This increase could result from the degradation of organic nitrogen with depth, where isotopically light $\delta^{15}\text{N}$ is preferentially released from the organic matrix, leaving behind isotopically heavier residual $\delta^{15}\text{N}$ (Saino and Hattori, 1980, 1987; Altabet, 1988). Similarly, the enrichment of $\delta^{15}\text{N}$ in SPM suggests that primary production mainly originates from autochthonous sources in some regions of the fjords (Figure 11). The horizontal-vertical distribution of the isotopic signal of $\delta^{13}\text{C}$ and $\delta^{15}\text{N}$ showed substantial variability in the northern Patagonian fjords. Our results strongly suggest that this variability was driven by biological processes, as was demonstrated by Savoye et al. (2003). In this work, the authors found that the co-variation of $\delta^{13}\text{C}$ and $\delta^{15}\text{N}$ reflect the seasonal succession of phytoplankton species due to seasonal changes in abiotic factors, such as temperature and nutrient concentration.

915 Silva and Vargas (2014) identified an LDOW zone near the fjord heads (<178 $\mu\text{mol L}^{-1}$), attributed to a significant influx of allochthonous particulate organic matter from local rivers (Figure 10). Nevertheless, the observed organic material mixture resulted in relatively lighter isotopic values of particulate organic matter than those expected for an autochthonous organic matter pool (Figure 7). Regardless, the input of organic matter (autochthonous or allochthonous) to the deep layer increased DO consumption through respiration, overwhelming the oxygen supply from horizontal advection (Figures 8 and 9).

920 The distribution of CDOM displayed distinct patterns within the Patagonian fjords (Figure 11). Higher CDOM concentrations were observed in the northern region and were attributed to factors such as greater terrestrial inputs, increased microbial activity, and longer residence times (Figure 13) of CDOM in these fjords (Mannino et al., 2008). In contrast, the southern region exhibited lower CDOM concentrations, indicating a decrease in dissolved terrestrial inputs and potentially more efficient removal processes. Localized increases in CDOM concentrations within specific fjords suggest the influence of local processes, such as freshwater inputs, glacial melting, or biological production, contributing to the heterogeneity of CDOM spatial distribution (Mannino et al., 2008).

925 The oceanic water masses (ESSW and SAAW) are strongly connected with the estuarine water masses (MSAAW and EW), as observed in this study (Figure 2). Organic matter degradation processes occurred inside the fjords, mainly in terms of nitrogenous compounds being remineralized, maintaining the nutrient pool that was originally transported by oceanic water, justifying the high accumulation of nitrate and phosphate registered in the subsurface layer of the Puyuhuapi Fjord and Jacaf Channel (Figure 3a-d). This process seems to be even more evident from the Jacaf Channel to the south (Figure 3), where it seems that organic matter was mostly retained and sedimented, which probably generated zones more prone to LDOW and hypoxia (Figure 2 and Figure 3).

930 At the fjord heads, where low salinity from high river freshwater inputs dominated, a persistent halocline/pycnocline/stratified water column developed; therefore, deep water ventilation by vertical mixing and diffusion with the oxic surface layer was limited (Figure 2-5). These conditions favored the occurrence of LDOW zones at the fjord, where stratification and particulate organic matter input were higher than at their mouths (Figure 9), thus favoring the consumption of DO due to organic matter degradation, as was reported in the Milford Sound in New Zealand (Stanton, 1984), Framvaren Fjord in Norway (Yao and Millero, 1995) and the Lower St. Lawrence Estuary in Canada (Lefort et al., 2012), as well as in the Reloncaví, Comau, Puyuhuapi, Aysén, and Quitrileo fjords (Figure 2).

945 **4.2. Mechanisms driving hypoxia and ~~LDOW deoxygenation~~ in northern Patagonian fjords**

950 As discussed in the previous section, one of the principal mechanisms involved in the origin of hypoxic conditions in some areas of the northern Patagonian fjords was attributed to the advection of the ESSW from the Pacific Ocean to Patagonia. Recently, Linford et al. (2023) demonstrated the poleward advection of water with lower DO values by the ESSW that was transported by the Perú Chile Undercurrent (PCUC). The passage of this water mass into the northern Patagonian fjord system was detected in a DO time series from a mooring system installed at the Guafo mouth. Moreover, as shown in Figure 2, extreme hypoxic conditions were registered in the Quitrileo Fjord, where ESSW was not delivered (Figure 4d-f).

In the Quitalco Fjord, the DO concentration was mainly governed by the biological processes of oxygen production and consumption during photosynthesis and respiration, respectively. The primary production experiments conducted in this fjord (Figure 7-8 and Figure 89) showed higher values of community respiration than the primary production of DO (Table 2). In addition, the oceanographic model showed a less intense deep net current, allowing a residence time of water between 100–150 days (Figures 11 and Figure 4213). Furthermore, satellite images provide evidence of highly suspended sediments along the Quitalco Fjord due to river discharge (Figure 910). Regarding Magdalena Sound, the shallower hypoxia observed there (70 m depth) could be explained by the occurrence of local upwelling produced when westerly winds blow across the mountains, as was reported for the Comau Fjord by Crosswell et al., (2022) and Díaz et al., (2023). A shallower hypoxia (10–20 m) was also registered in Clayoquot Sound, British Columbia, mainly attributed to the local processes, such as, DO consumption during the organic matter degradation, enhanced by upwelling conditions (Rosen et al., 2022).

DO produced by photosynthesis is primarily depleted through respiration; therefore, in many oceanic environments, the GPP and CR rates tend to be tightly coupled. However, in coastal waters or fjord ecosystems, owing to the high amount of organic matter (autochthonous and allochthonous) available in the water column, a greater amount of oxygen is consumed (Jackson et al., 2022) during microbial respiration (Robinson, 2019), thus dominating heterotrophic processes over autotrophic processes. This study recorded high CR rates (greater than GPP), indicating heterotrophic metabolism, where more oxygen was consumed than produced (Figure 78). Nevertheless, Puyuhuapi Fjord, Reloncaví Fjord, and Compu estuary fjords always showed high oxygen production values ($GPP > 20 \text{ mmol O}_2 \text{ m}^{-3} \text{ d}^{-1}$) at within the 2 to 4 m layer at least in one of the two sampling depth (Figure 8), confirming suggesting that a greater uptake than release of Patagonian fjords act as a net sink of atmospheric CO₂ due to the high surface primary production rates during the spring-summer period at surface waters of some Patagonian fjords (Torres et al., 2011). A recent global assessment of CO₂ uptake from estuaries, including tidal systems and deltas, lagoons, and fjord reported that fjords ecosystems can reduce 37% of CO₂ emissions (Rosentreter et al., 2023). DO and organic matter are produced only in the well-lit upper ocean but can be consumed throughout the water column. Therefore, in areas of high surface production and slow resupply of oxygen at depth (compared to the rate at which oxygen is respired), DO concentrations may be reduced to hypoxic levels at depth. Nevertheless, deepwater renewal was observed in Puyuhuapi Fjord owing to the inflow of salty water above the sill favoring the ventilation of the intermediate layer and inhibiting the occurrence of deep anoxia conditions (Pinilla et al., 2020), as was also reported by Jackson et al., (2022) in Rivers Inlet, British Columbia.

However, the first map of residence time in the northern Patagonian fjord showed a coincidence of the area where a high residence time was reported (100–250 days, Figure 4213) with the depleted oxygen region, for example, hypoxic and LDOW areas (Figure 2). The hydrodynamic model and derived calculations are helpful tools for explaining the oxygen distribution and patterns in the northern Patagonian fjord system.

Deoxygenation of subsurface water (50–200 m depth) was detected in Puyuhuapi Fjord when *in situ* DO profiles were compared with a time difference of 50 years, reporting negative values $\Delta DO = 30\text{--}40 \mu\text{mol L}^{-1}$ (Figure 6). Linford et al. (2023) provided an explanation for deoxygenation in Patagonian waters. The leading causes were the increase in the poleward transport of the PCUC and the consequent increase in the advection of the ESSW to the

990 Patagonian. Moreover, as presented in this manuscript, we also included evidence of the biological physical processes (DO consumption during respiration, lower ventilation, and suspended sediment supply) as one of the other processes contributing to deoxygenation in Patagonian fjords. In addition, an increase in inorganic nutrients, e.g., NO_3^- and PO_4^- of 2 μM and 0.5 μM was also registered in the last 50 years, possibly due to the increase in the primary production or as a response to anthropogenic activities, e.g., salmon and mussel aquaculture. However, further investigation is necessary to quantify the impact of these economic activities on the deoxygenation process.

5. Conclusions

995 Since the beginning of oceanographic research in the Patagonian fjords (1970), hypoxia and LDOW have been reported along the water column. A dataset of hydrographic-biogeochemical parameters, *in-situ* experiments of primary production/community respiration, satellite-suspended sediments, and the output of a hydrodynamic model allowed for the first time the scrutinization quantification of the oceanographic and biogeochemical processes contributing to the hypoxia and LDOW-deoxygenation of the Patagonian subsurface waters. The influence of the ESSW was recognized as one of the first drivers of this phenomenon. This water mass transported poleward poorly oxygenated waters that entered the northern Patagonian fjords through the Guafo mouth and moved southward through the Moraleda and Jacaf channels and the Puyuhuapi Fjord. The distribution of the ESSW inside the northern Patagonian fjords coincides with the most extensive zone of the LDOW records. However, the hypoxic conditions registered in this zone were also attributed to the high rate of DO consumption during community respiration processes, owing to the entrance of allochthonous organic matter (natural and/or anthropogenic) to the fjords. Additionally, the results from marine currents derived from ADCP measurements and the hydrodynamic model demonstrated a weak water circulation and a long residence time contributing to the reduction of deep-water ventilation, resulting in a drop in DO level, and finally, the occurrence of hypoxic conditions.

1010 The Quitralco Fjord also reported hypoxic conditions showing the absolute minimum of DO with 9.36 $\mu\text{mol L}^{-1}$ and 1.6% oxygen saturation. ESSW was not observed in this area. Therefore, the presence of hypoxic water in the deep layer of Quitralco was attributed to weak deep-water circulation and a long residence time, together with a high rate of DO consumption by community respiration and a higher supply of allochthonous organic matter due to river discharge. Similar processes favoring LDOW were registered at the Aysén, Comau, and Reloncaví fjords, but in the Reloncaví systems, marine currents and residence time were significantly higher than in other fjords. The presence of LDOW in the Reloncaví systems responded mainly to biological processes, e.g., DO consumption during the primary production community respiration by phytoplankton, and secondary production remineralization by bacteria.

1020 The analyses Quantification of the processes contributing to hypoxic conditions and LDOW in the water column of northern Patagonian fjords allowed for the identification of the main causes favoring the oxygen loss deoxygenation of each fjord investigated. The results provide the environmental information needed to contribute to the sustainable management of the northern Patagonian fjord under anthropogenic activities and climate change scenarios. In addition, it provides significant information for understanding the life cycle of marine species that inhabit Patagonian fjords.

1025 Finally, our study provides valuable insights into the relationship between hypoxia, low oxygen processes,
the origin of organic carbon, isotopic signals of carbon and nitrogen, the C:N ratio, and the presence of CDOM in
the Patagonian fjords. These findings highlight the complex interactions between terrestrial and marine processes
and emphasize the role of fjords as potential sites for hypoxia and the accumulation of organic matter.
1030 Understanding these relationships is crucial for accurately assessing the impact of low oxygen processes and carbon
cycle dynamics in fjord ecosystems and their contribution to the global carbon cycle. Further research is needed to
elucidate the mechanisms driving these patterns and their implications for the functioning and resilience of fjord
ecosystems against continuous environmental changes.

Data availability. All data sets used in this manuscript can be requested from the corresponding author.

1035 *Author contributions.* PL: study design, data analysis, and manuscript leader. IPS: study design, collection, and
analysis of physical oceanographic data, and manuscript leader. PM: study design, collection, and analysis of
primary production data. PD: study design, collection, and analysis of physical-biological oceanographic data. CA:
collection, and analysis of primary production data. EP: developed of oceanographic model and analysis of physical
oceanographic data. FB: collection, and analysis of biogeochemical data. MC: analysis of marine current data. AA:
1040 study design, collection, and analysis of satellite data. MA: collection and analysis of marine current data. GS: study
design, collection, and analysis of physical oceanographic data. CP: edition and analysis of satellite data. CS:
collection, and analysis of physical oceanographic data. SA: collection, and analysis of biogeochemical data. PN:
collection, and analysis of biogeochemical data. GM: collection of physical, biological, and biogeochemical data.
RA: collection of physical, biological, and biogeochemical data. JSM: processing and analysis of model data for
1045 resident time. CSR: validation hydrodynamics model. All authors contributed to the writing of the manuscript.

Competing interests. The authors declare that they have no conflict of interest.

Acknowledgments.

1050 This research was funded by COPAS Sur-Austral ANID AFB170006, the Office of Naval Research grant N00014-
17-1-2606, COPAS COASTAL FB210021, and CIEP R20F002. Iván Pérez-Santos was also funded by
FONDECYT 1211037. Facundo Barrera was founded by FONDECYT 31308. Cécile Pujol was financially
supported by the F.R.S-FNRS (Fonds de la Recherche Scientifique de Belgique, Communauté Française de
Belgique) through a FRIA grant. Patricio A. Díaz was funded by Centre for Biotechnology and Bioengineering
1055 (CeBiB) (PIA project FB0001, ANID, Chile). M.I. Castillo was funded by CS2018-7929 and ATE220033. We also
thank the Chonos initiative of the Instituto de Fomento Pesquero (IFOP) for facilitating the use of its computer
systems to access the MIKE 3, WRF, and FLOW models and the Ministry of Economy, Development and Tourism
of the Chilean Government for funding through the Undersecretary of Fisheries and Aquaculture. Elias Pinilla
would like to acknowledge funding from the National Science Foundation (NSF Grant Number 2045866).

1060

Reference

Andrejev, O., Myrberg, K., and Lundberg, P. A.: Age and renewal time of water masses in a semi-enclosed basin—application to the Gulf of Finland, *Tellus A: Dynamic Meteorology and Oceanography*, 56, 5–, 548-558, doi:10.3402/tellusa.v56i5.14435, 2004.

1065 [Altabet, M.A.: Variations in nitrogen isotopic composition between sinking and suspended particles: implication for nitrogen cycling and particle transformation in the open ocean. *Deep-Sea Res.* 35, 535–554, 1988.](#)

Andrewartha, H. G., and Birch, L. C.: *The ecological web: more on the distribution and abundance of animals*, University of Chicago Press, 1986.

1070 Barrera, F., Lara, R., Krock, J., Factors influencing characteristics and distribution of organic particles and macromolecules in the Pacific-Atlantic connection, *J. Mar. Syst.*, 175, 36-45, doi:10.1016/j.jmarsys.2017.07.004, 2017.

Batiuk, R. A., Breitburg, D. L., Diaz, R. J., Cronin, T. M., Secor, D. H., and Thursby, G.: Derivation of habitat-specific dissolved oxygen criteria for Chesapeake Bay and its tidal tributaries, *Journal of Experimental Marine Biology and Ecology*, 381, S204-S215, doi:10.1016/j.jembe.2009.07.023, 2009.

1075 Bianchi, T. S.: *Biogeochemistry of estuaries*. Oxford University Press on Demand, 2007.

Billi, M., Mascareño, A., Henríquez, P. A., Rodríguez, I., Padilla, F., and Ruz, G. A.: Learning from crises? The long and winding road of the salmon industry in Chiloé Island, Chile, *Marine Policy*, 140, 105069, doi:10.16/j.marpol.2022.105069, 2022.

1080 Breitburg, D. L., Loher, T., Pacey, C. A., and Gerstein, A.: Varying effects of low dissolved oxygen on trophic interactions in an estuarine food web, *Ecological Monographs*, 67, 4, 489-507, doi:10.1890/0012-9615(1997)067[0489:VEOLDO]2.0.CO;2, 1997.

Breitburg, D., Levin, L. A., Oschlies, A., Grégoire, M., Chavez, F. P., Conley, D. J., ... and Zhang, J.: Declining oxygen in the global ocean and coastal waters, *Science*, 359, 6371, doi:10.1126/science.aam7240, 2018.

1085 Castillo, M. I., Cifuentes, U., Pizarro, O., Djurfeldt, L., and Caceres, M.: Seasonal hydrography and surface outflow in a fjord with a deep sill: the Reloncaví fjord, Chile, *Ocean Science*, 12, 2, 533-544, doi:10.5194/os-12-533-2016, 2016.

[Carrasco, C., Silva, N.: Comparación de las características oceanográficas físicas y químicas presente en la zona de Puerto Montt a la boca del Guafo entre el invierno y la primavera de 2004 y entre las primaveras de 1995 y 2004. *Cienc. Tecnol. del Mar* 33 \(2\), 17–44, 2010.](#)

1090 Conley, D. J., Paerl, H. W., Howarth, R. W., Boesch, D. F., Seitzinger, S. P., Havens, K. E., ... and Likens, G. E.: Controlling eutrophication: nitrogen and phosphorus, *Science*, 323, 5917, 1014-1015, doi:10.1126/science.1167755, 2009.

[Colin A. S., Norman B. N.: Chapter 10 - The Optical Properties of DOM in the Ocean, Editor\(s\): Dennis A. Hansell, Craig A. Carlson, *Biogeochemistry of Marine Dissolved Organic Matter \(Second Edition\)*, Academic Press, 2015, Pages 481-508, ISBN 9780124059405, <https://doi.org/10.1016/B978-0-12-405940-5.00010-8>, 2015.](#)

1095

- Crosswell, J.R., Bravo, F., Pérez-Santos, I., Carlin, G., Cherukuru, N., Schwarger, C., et al.: Geophysical controls on metabolic cycling in three Patagonian fjords. *Prog. Oceanogr.* 207, 102866, 2022.
- Davis, J. C.: Minimal dissolved oxygen requirements of aquatic life with emphasis on Canadian species: a review, *Journal of the Fisheries Board of Canada*, 32, 12, 2295-2332, doi:10.1139/f75-268, 1975.
- 1100 Diaz, R. J., and Rosenberg, R.: Marine benthic hypoxia: a review of its ecological effects and the behavioural responses of benthic macrofauna, *Oceanography and marine biology, An annual review*, 33, 245, 03, 1995.
- Diaz, R. J.: Overview of hypoxia around the world, *Journal of environmental quality*, 30, 2, 275-281, doi:10.2134/jeq2001.302275x, 2001.
- 1105 [Díaz, P., Pérez-Santos, I., Álvarez, G., Garreaud, R., Pinilla, E., Díaz, M., Sandoval, A., Araya, M., Álvarez, F., Rengel, J., Montero, P., Pizarro, G., López, L., Iriarte, L., Igor, G., Reguera, B.: Multiscale physical background to an exceptional harmful algal bloom of *Dinophysis acuta* in a fjord system. *Sci. Total Environ.* 773, 145621 <https://doi.org/10.1016/j.scitotenv.2021.145621>, 2021.](#)
- Díaz, P. A., Pérez-Santos, I., Basti, L., Garreaud, R., Pinilla, E., Barrera, F., ... and Figueroa, R. I.: The impact of local and climate change drivers on the formation, dynamics, and potential recurrence of a massive fish-killing microalgal bloom in Patagonian fjord, *Science of The Total Environment*, 865, 161288, doi:10.16/j.scitotenv.2022.161288, 2023.
- 1110 [DHI: Mike 3. User Guide and Reference Manual. Danish Hydraulic Institute, Denmark, 2019.](#)
- Ekau, W., Auel, H., Pörtner, H. O., and Gilbert, D.: Impacts of hypoxia on the structure and processes in pelagic communities (zooplankton, macro-invertebrates and fish), *Biogeosciences*, 7, 5, doi:10.5194/bg-7-1669-2010, 1669-1699, 2010.
- 1115 Fuenzalida, R., Schneider, W., Garcés-Vargas, J., Bravo, L., and Lange, C. : Vertical and horizontal extension of the oxygen minimum zone in the eastern South Pacific Ocean, *Deep Sea Research Part II: Topical Studies in Oceanography*, 56, 16, 992-1003, doi:10.1016/j.dsr2.2008.11.001, 2009.
- [Fry, B., and Sherr, E. B.: \$\delta^{13}C\$ measurements as indicators of carbon flow in marine and freshwater ecosystems. *Ecol. Stud.* 68, 196–229. doi: 10.1007/978-1-4612-3498-2_12, 1989.](#)
- 1120 Garçon V., Dewitte B., Goubanova C. and Montes I.: Land-sea-atmosphere interactions exacerbating ocean deoxygenation in Eastern Boundary Upwelling Systems (EBUS), in 'Laffoley, D. and Baxter, J.M. (eds.). *Ocean deoxygenation: Everyone's problem - Causes, impacts, consequences and solutions*, Gland, Switzerland: IUCN. xxii+562pp, available at: <https://portals.iucn.org/library/sites/library/files/documents/03.420 DEOX.Pdf>, 2019.
- 1125 González, H. E., Calderón, M. J., Castro, L., Clement, A., Cuevas, L. A., Daneri, G., ... and Molinet, C.: Primary production and plankton dynamics in the Reloncaví Fjord and the Interior Sea of Chiloé, Northern Patagonia, Chile, *Marine Ecology Progress Series*, 402, 13-30, doi:10.3354/meps08360, 2010.
- González, H. E., Nimptsch, J., Giesecke, R., and Silva, N.: Organic matter distribution, composition and its possible fate in the Chilean North-Patagonian estuarine system, *Science of the Total Environment*, 657, 1419-1431, doi:10.1016/j.scitotenv.2018.11.445, 2019.
- 1130 Grasshoff, K., Ehrhardt, M., and Kremling, K. *Methods of Seawater Analysis*. (2nd edition), Verlag Chemie Weinheim, New York, USA, 1983.

- Grasshoff, K., Kremling, K., and Ehrhardt, M. (Eds.): *Methods of seawater analysis*, John Wiley and Sons, 2009.
- 1135 [Harmelin-Vivien, M., Loizeau, V., Mellon, C., Beker, B., Arlhac, D., Bodiguel, X., et al.: Comparison of C and N stable isotope ratios between surface particulate organic matter and microphytoplankton in the Gulf of lions \(NW Mediterranean\). *Cont. Shelf Res.* 28, 1911–1919. doi: 10.1016/j.csr.2008.03.002, 2008.](#)
- Herrmann, R. B.: *Growth of juvenile coho salmon at various concentrations of dissolved oxygen*, 1958.
- Hoos, L.M.: *A study of the benthos of an anoxic marine basin and factors affecting its distribution*, M. Sc. Thesis, Dalhousie University, Halifax, NS. 149, 1973.
- 1140 [Holding, J.M., Duarte, C.M., Delgado-Huertas, A., Soetaert, K., Vonk, J.E., Agustí, S., Wassmann, P. and Middelburg, J.J.: Autochthonous and allochthonous contributions of organic carbon to microbial food webs in Svalbard fjords. *Limnol. Oceanogr.*, 62: 1307-1323. <https://doi.org/10.1002/lno.10526>, 2017.](#)
- [Guzmán D & Silva N.: Caracterización física y química y masas de agua en los canales australes de Chile entre boca del Guafo y estero Elefantes \(crucero CIMAR 4 Fiordos\). *Cienc. Tecnol. Mar.* 25\(2\): 45-76, 2002.](#)
- 1145 IOC, S.: IAPSO: The international thermodynamic equation of seawater–2010: Calculation and use of thermodynamic properties, Intergovernmental Oceanographic Commission, Manuals and Guides No. 56, UNESCO, Manuals and Guides, 56, 1-196, 2010.
- Iriarte, J. L.: Natural and human influences on marine processes in Patagonian Subantarctic coastal waters, *Frontiers in Marine Science*, 5, 360, doi:10.3389/fmars.2018.00360, 2018.
- 1150 [Iriarte, J.L., Gonzalez, H.E., Liu, K.K., Rivas, C., Valenzuela, C.P.: Spatial and temporal variability of chlorophyll and primary productivity in surface waters of southern Chile. *Estuarine. Coast. Shelf Sci.* 74, 471e480, 2017.](#)
- Kattner, G., and Becker, H.: Nutrients and organic nitrogenous compounds in the marginal ice zone of the Fram Strait, *Journal of Marine Systems*, 2, 3-4, 385-394, doi:10.1016/0924-7963(91)90043-T, 1991.
- [Jackson, J. M. Johannessen S., Belluz J., Hunt B., Hannah C.: Identification of a Seasonal Subsurface Oxygen Minimum in Rivers Inlet, British Columbia, *Estuaries and Coasts*, 45:754–771, <https://doi.org/10.1007/s12237-021-00999-y>, 2022.](#)
- [Kumar, V., Tiwari, M., Nagoji, S. et al.: Evidence of Anomalously Low \$\delta^{13}\text{C}\$ of Marine Organic Matter in an Arctic Fjord. *Sci Rep* 6, 36192. <https://doi.org/10.1038/srep36192>, 2016.](#)
- 1160 [Kuliński, K., Kedra, M., Legeżyńska, J., Gluchowska, M., & Zaborska, A.: Particulate organic matter sinks and sources in high Arctic fjord. *Journal of Marine Systems*, 139, 27–37. doi:10.1016/j.jmarsys. 2014.04.018, 2014.](#)
- Kutty, M. N.: Respiratory quotients in goldfish and rainbow trout, *Journal of the Fisheries Board of Canada*, 25, 8, 1689-1728, doi:10.1139/f68-150, 1968.
- Laffoley, D., and Baxter, J. M.: *Ocean deoxygenation: Everyone's problem-Causes, impacts, consequences and solutions*, Gland, Switzerland: IUCN, doi:10.2305/IUCN.CH.2019.13.en, 2019.
- 1165 Lefort, S.: *A multidisciplinary study of hypoxia in the deep water of the Estuary and Gulf of St. Lawrence: Is this ecosystem on borrowed time?*, McGill University (Canada), 2012.
- [Linford, P., Pérez-Santos, I., Montes, I., Dewitte, B., Buchan, S., Narváez, D., Saldías, G., Pinilla, E., Garreaud, R., Díaz, P., Schwerter, C., Montero, P., Rodríguez-Villegas, C., Cáceres Soto, M., Mancilla-Gutiérrez, G., and Altamirano R.: Recent Deoxygenation of Patagonian Fjord Subsurface Waters Connected to the Peru Chile](#)

- 1170 Undercurrent and Equatorial Subsurface Water Variability. Submitted to Global Biogeochemical cycles (Under review), 2023.
- Linford, P., Pérez-Santos, I., Montes, I., Dewitte, B., Buchan, S., Narváez, D., et al.: Recent deoxygenation of Patagonian fjord subsurface waters connected to the Peru–Chile undercurrent and equatorial subsurface water variability. *Global Biogeochemical Cycles*, 37, e2022GB007688. <https://doi.org/10.1029/2022GB007688>. 2023.
- 1175 Mannino A., Russ M. E., Hooker S. B.: Algorithm development and validation for satellite-derived distributions of DOC and CDOM in the U.S. Middle Atlantic Bight, *J. Geophys. Res.*, 113, C07051, doi:10.1029/2007JC004493, 2008.
- Martínez, D., De Lázaro, O., Cortés, P., Oyarzún-Salazar, R., Paschke, K., and Vargas-Chacoff, L.: Hypoxia modulates the transcriptional immunological response in *Oncorhynchus kisutch*, *Fish and Shellfish Immunology*, 106, 1042-1051, doi:10.16/j.fsi.2020.09.025, 2020.
- 1180 Mardones, J.I., Paredes, J., Godoy, M., Suarez, R., Norambuena, L., Vargas, V., Fuenzalida, G., Pinilla, E., Artal, O., Rojas, X., Dorantes-Aranda, J.J., Lee Chang, K.J., Anderson, D.M., Hallegraeff, G.M.: Disentangling the environmental processes responsible for the world’s largest farmed fish-killing harmful algal bloom: Chile, 2016. *Sci. Total Environ.* 766, 144383 <https://doi.org/10.1016/j.2021>.
- 1185 Meire, L. K. E. R., Soetaert, K. E. R., and Meysman, F. J. R.: Impact of global change on coastal oxygen dynamics and risk of hypoxia, *Biogeosciences*, 10, 4, 2633-2653, doi:10.5194/bg-10-2633-2013, 2013.
- Monsen, N. E., Cloern, J. E., Lucas, L. V., and Monismith, S. G.: A comment on the use of flushing time, residence time, and age as transport time scales, *Limnology and oceanography*, 47, 5, 1545-1553, doi:10.4319/lo.2002.47.5.1545, 2002.
- 1190 Montero, P., Daneri, G., Gonzalez, H. E., Iriarte, J. L., Tapia, F. J., Lizarraga, L., ... and Pizarro, O.: Seasonal variability of primary production in a fjord ecosystem of the Chilean Patagonia: Implications for the transfer of carbon within pelagic food webs, *Continental Shelf Research*, 31, 3-4, 202-215, doi:10.1016/j.csr.2010.09.003, 2011.
- 1195 Montero, P., Pérez-Santos, I., Daneri, G., Gutiérrez, M. H., Igor, G., Seguel, R., ... and Crawford, D. W.: A winter dinoflagellate bloom drives high rates of primary production in a Patagonian fjord ecosystem, *Estuarine, Coastal and Shelf Science*, 199, 105-116, doi:10.3856/vol45-issue5-fulltext-16, 2017.
- Montero, P., Daneri, G., Tapia, F., Iriarte, J. L., and Crawford, D.: Diatom blooms and primary production in a channel ecosystem of central Patagonia, *Lat. Am. J. Aquat. Res.* 45, 999–1016, doi: 10.3856/vol45-issue5-fulltext-16, 2017a.
- 1200 Montero, P., Gutiérrez, M. H., Daneri, G., and Jacob, B.: The Effect of Salmon Food-Derived DOM and Glacial Melting on Activity and Diversity of Free-Living Bacterioplankton in Chilean Patagonian Fjords, *Frontiers in Microbiology*, 12, 772900, doi:10.3389/fmicb.2021.772900, 2022
- 1205 -Muñoz P, J Sellanes, K Villalobos, G Zapata-Hernández, C Mayr & K Araya.: Geochemistry of reduced fluids from shallow cold vents hosting chemosynthetic communities (Comau Fjord, Chilean Patagonia, 42°S). *Progress in Oceanography* 129: 159-169, 2014.

- Nechad, B., Dogliotti, A., Ruddick, K., and Doxaran, D.: Particulate backscattering and suspended matter concentration retrieval from remote-sensed turbidity in various coastal and riverine turbid waters, In Living Planet Symposium, Proceedings of the conference held, 9-13, 2016.
- 1210 Nimpfisch, J., Woelfl, S., Osorio, S., Valenzuela, J., Ebersbach, P., von Tuempling, W., ... and Graeber, D.: Tracing dissolved organic matter (DOM) from land-based aquaculture systems in North Patagonian streams, *Science of the Total Environment*, 537, 129-138, doi:10.1016/j.scitotenv.2015.07.160, 2015.
- Oschlies, A., Brandt, P., Stramma, L., and Schmidtko, S.: Drivers and mechanisms of ocean deoxygenation, *Nature Geoscience*, 11, 7, 467-473, doi:10.1038/s41561-018-0152-1, 2018.
- Paulmier, A., and Ruiz-Pino, D.: Oxygen minimum zones (OMZs) in the modern ocean, *Progress in Oceanography*, 80, 3-4, 113-128, doi:10.1016/j.pocean.2008.08.001, 2009.
- 1215 [Pawłowicz, R., Beardsley, B., Lentz, S.: Classical tidal harmonic analysis including error estimates in MATLAB using T TIDE. *Comput. Geosci.* 28, 929–937. \[https://doi.org/10.1016/S0098-3004\\(02\\)00013-4\]\(https://doi.org/10.1016/S0098-3004\(02\)00013-4\), 2002.](#)
- Pérez-Santos, I., Garcés-Vargas, J., Schneider, W., Ross, L., Parra, S., and Valle-Levinson, A.: Double-diffusive layering and mixing in Patagonian fjords, *Progress in Oceanography*, 129, 35-49, doi:10.1016/j.pocean.2014.03.012, 1220 2014.
- Pérez-Santos, I., Castro, L., Ross, L., Niklitschek, E., Mayorga, N., Cubillos, L., ... and Daneri, G.: Turbulence and hypoxia contribute to dense biological scattering layers in a Patagonian fjord system, *Ocean Science*, 14, 5, 1185-1206, doi:10.5194/os-14-1185-2018, 2018.
- 1225 [Pérez-Santos, I., Díaz, P., Silva, N., Garreaud, R., Montero, P., Henríquez-Castillo, C., Barrera, F., Linford, P., Amaya, C., Contreras, S., Aracena, C., Pinilla, E., Altamirano, R., Vallejos, L., Pavez, J., Maulen, J.: *Oceanography time series reveals annual asynchrony input between oceanic and estuarine waters in Patagonian fjords. *Sci. Total Environ.* 798, 149241. doi.org/10.1016/j.scitotenv.2021.149241, 2021.*](#)
- Pinilla, E., Castillo, M. I., Pérez-Santos, I., Venegas, O., and Valle-Levinson, A.: Water age variability in a Patagonian fjord, *Journal of Marine Systems*, 210, 103376, doi:10.1016/j.jmarsys.2020.103376, 2020.
- 1230 [Pinilla, E., Soto, G., Arriagada, M., Canon, H.: *Diseño y estudio técnico de macrozonas de agrupaciones de concesiones en la zona sur austral X a XII Regiones. Valparaíso, Instituto de Fomento Pesquero. Available: \[http://190.151.20.106/exlibris/aleph/a23_1/apache_media/VB3VMRJKVR6S2C2IA2E1XGA85FOPPC.pdf\]\(http://190.151.20.106/exlibris/aleph/a23_1/apache_media/VB3VMRJKVR6S2C2IA2E1XGA85FOPPC.pdf\), 2012.*](#)
- Prandle, D.: Simple theory for designing tidal power schemes, *Advances in water resources*, 7, 1, 21-27, doi:10.1016/0309-1708(84)90026-5, 1984.
- 1235 [Pryer HV, Hawkings JR, Wadham JL, Robinson LF, Hendry KR, Hatton JE, Kellerman AM, Bertrand S, Gill-Olivas B, Marshall MG, Brooker RA, Daneri G, Häussermann V.: *The Influence of Glacial Cover on Riverine Silicon and Iron Exports in Chilean Patagonia. *Global Biogeochem Cycles*, Dec;34\(12\):e2020GB006611. doi: 10.1029/2020GB006611. Epub 2020 Dec 17. PMID: 33519063; PMCID: PMC7818384, 2020.*](#)
- 1240 Quiñones, R. A., Fuentes, M., Montes, R. M., Soto, D., and León-Muñoz, J.: Environmental issues in Chilean salmon farming: a review, *Reviews in Aquaculture*, 11, 2, 375-402, doi:10.1111/raq.12337, 2019.
- Remeikaitė-Nikienė, N., Lujanienė, G., Malejevas, V., Barisevičiūtė, R., Zilius, M., Vybernaitė-Lubienė, I., ... and Stankevičius, A.: Assessing nature and dynamics of POM in transitional environment (the Curonian Lagoon, SE

- Baltic Sea) using a stable isotope approach, *Ecological Indicators*, 82, 217-226, doi:10.1016/j.ecolind.2017.06.035, 2017.
- 1245 [Reche, P., Artal, O., Pinilla, E., Ruiz, C., Venegas, O., Arriagada, A., Falvey, M.: CHONOS: oceanographic information website for Chilean Patagonia. *Ocean Coast Manag.* 208, 105634 <https://doi.org/10.1016/j.ocecoaman.2021.105634>, 2021.](#)
- [Redfield A. C.: The biological control of chemical factors in the environment. *Am. Sci.*, 46:230A-A221, 1958.](#)
- 1250 [Robinson, C.: Microbial respiration, the engine of ocean deoxygenation, *Frontiers in Marine Science*, 5, 533, doi:10.3389/fmars.2018.00533, 2019.](#)
- [Rodi, W: In: *Turbulence Models and Their Application in Hydraulics*. Delft, p. 104, 1984.](#)
- [Rosentreter et al.: Coastal vegetation and estuaries are collectively a greenhouse gas sink. *Nature climate change*. <https://doi.org/10.1038/s41558-023-01682-9>, 2023.](#)
- 1255 [Rosen S., Bianucci L., Jackson J.M., Hare A., Greengrove C., Monks R., Bartlett M. and Dick J.: Seasonal near-surface hypoxia in a temperate fjord in Clayoquot Sound, British Columbia. *Front. Mar. Sci.* 9:1000041. doi: 10.3389/fmars.2022.1000041, 2022.](#)
- [Ruiz, C., Artal, O., Pinilla, E., and Sepúlveda, H. H.: Stratification and mixing in the Chilean Inland Sea using an operational model, *Ocean Modelling*, 158, 101750, doi:10.1016/j.ocemod.2020.101750, 2021.](#)
- 1260 [Sampaio, E., Santos, C., Rosa, I. C., Ferreira, V., Pörtner, H. O., Duarte, C. M., ... and Rosa, R.: Impacts of hypoxic events surpass those of future ocean warming and acidification, *Nature Ecology and Evolution*, 5, 3, 311-321, doi:10.1038/s41559-020-01370-3, 2021.](#)
- [Saino, T., Hattori, A.: 15N natural abundance in oceanic suspended particulate matter. *Nature* 283, 752-754, 1980.](#)
- 1265 [Saino, T., Hattori, A.: Geographical variation of the water column distribution of suspended particulate nitrogen and its 15N natural abundance in the Pacific and its marginal seas. *Deep-Sea Res.* 34, 807-827, 1987.](#)
- [Savoye N, Aminot A, Treguer P, Fontugne M, Naulet N, K erouel R.: Dynamics of particulate organic matter \$\delta^{15}\text{N}\$ and \$\delta^{13}\text{C}\$ during spring phytoplankton blooms in a macrotidal ecosystem \(Bay of Seine, France\). *Mar Ecol-Progr Ser* 255:27-41, 2003.](#)
- [Schmidtko, S., Stramma, L., and Visbeck, M.: Decline in global oceanic oxygen content during the past five decades, *Nature*, 542, 7641, 335-339, doi:10.1038/nature21399, 2017.](#)
- 1270 [Schneider, W., P rez-Santos, I., Ross, L., Bravo, L., Seguel, R., and Hern andez, F.: On the hydrography of Puyuhuapi Channel, Chilean Patagonia, *Progress in Oceanography*, 129, 8-18, doi:10.1016/j.pocean.2014.03.007, 2014.](#)
- 1275 [Schneider, B., Schlitzer, R., Fischer, G. & Nothig, E. M.: Depth-dependent elemental compositions of particulate organic matter \(POM\) in the ocean. *Glob. Biogeochem. Cycle* <https://doi.org/10.1029/2002gb001871>, 2003.](#)
- [Sibson, R., and Thomson, G. D.: A seamed quadratic element for contouring, *The Computer Journal*, 24, 4, 378-382, doi:10.1093/comjnl/24.4.378, 1981.](#)
- 1280 [Sievers, H. A.: Temperature and salinity in the austral Chilean channels and fjords. Progress in the oceanographic knowledge of Chilean interior waters, from Puerto Montt to Cape Horn. Comit  Oceanogr fico Nacional-Pontificia Universidad Cat lica de Valpara so, Valpara so, 31-36, 2008.](#)

- Sievers, A.H. and N. Silva.: Water masses and circulation in austral Chilean channels and fjords, In: N. Silva and S. Palma (eds.), Progress in the oceanographic knowledge of Chilean inner waters, from Puerto Montt to Cape Horn, Comité Oceanográfico Nacional, Pontificia Universidad Católica de Valparaíso, Valparaíso, pp. 53-58. <http://www.cona.cl/>, 2008.
- 1285 Silva, N.: Physical and chemical characteristics of the surface sediments in the austral Chilean channels and fjords, Progress in the oceanographic knowledge of Chilean interior waters, from Puerto Montt to Cape Horn, 69-75, <http://www.cona.mil.cl/>, 2008.
- Silva, N., Rojas, N., and Fedele, A.: Water masses in the Humboldt Current System: Properties, distribution, and the nitrate deficit as a chemical water mass tracer for Equatorial Subsurface Water off Chile, Deep Sea Research Part II: Topical Studies in Oceanography, 56, 16, 1004-1020, doi:10.1016/j.dsr2.2008.12.013, 2009.
- 1290 [Thomson, R.E., Emery, W.J.: Data Analysis Methods in Physical Oceanography, Elsevier, Waltham, Mass. Paperback ISBN: 9780123877826, 2014.](#)
- Silva, N., and Vargas, C. A.: Hypoxia in Chilean patagonian fjords, Progress in Oceanography, 129, 62-74, doi:10.1016/j.pocean.2014.05.016, 2014.
- 1295 Smith, D. C., and Azam, F.: A simple, economical method for measuring bacterial protein synthesis rates in seawater using 3H-leucine, Mar. Microb. food webs, 6, 2, 107-114, 1992.
- [Sibson, R.: A Brief Description of Natural Neighbor Interpolation. In: Barnett, V., Ed., Interpreting Multivariate Data, John Wiley & Sons, New York, 21-36, 1981.](#)
- Soto, D., and Norambuena, F.: Evaluation of salmon farming effects on marine systems in the inner seas of southern Chile: a large-scale mensurative experiment, Journal of Applied Ichthyology, 20, 6, 493-501, doi:10.1111/j.1439-0426.2004.00602, 2004.
- 1300 Soto, D., León-Muñoz, J., Garreaud, R., Quiñones, R. A., and Morey, F.: Scientific warnings could help to reduce farmed salmon mortality due to harmful algal blooms, Marine Policy, 132, 104705, doi:10.16/j.marpol.2021.104705, 2021.
- 1305 [Soto-Riquelme, C., Pinilla E., Ross L.: Wind influence on residual circulation in Patagonian channels and fjords, Continental Shelf Research 254, 104905, 2023.](#)
- [Skamarock, W.C., Klemp, J.B., Dudhia, J., Gill, D.O., Barker, D.M., Duda, M.G., Huang, X.-Y., Wang, W., Powers, J.G.: A description of the advanced research WRF version 3. NCAR Technical Note 475, 125, 2008.](#)
- [Smagorinsky, J.: General circulation experiments with the primitive equations. Mon. Wea. Rev., 91, 99–164, 1963.](#)
- 1310 Stanton, B. R.: Some oceanographic observations in the New Zealand fjords, Estuarine, coastal and shelf science, 19, 1, 89-104, doi:10.1016/0272-7714(84)90054-4, 1984.
- Strickland, J. D. H.: Measuring the production of marine phytoplankton, Fish. Res. Bd. Canada Bull., 122, 172, 1960.
- Strickland, J. D. H., and Parsons, T. E.: Determination of dissolved oxygen, A practical handbook of seawater analysis, 167, 71-75, 1968.
- 1315 Takeoka, H.: Fundamental concepts of exchange and transport time scales in a coastal sea, Continental Shelf Research, 3, 3, 311-326, doi:10.1016/0278-4343(84)90014-1, 1984.

- 1320 [Taucher, J., Boxhammer, T., Bach, L. T., Paul, A. J., Schartau, M., Stange, P., & Riebesell, U.: Changing carbon-to-nitrogen ratios of organic-matter export under ocean acidification. *Nature Climate Change*. doi:10.1038/s41558-020-00915-5, 2020.](#)
- Tomas, C. R. (Ed.): Identifying marine phytoplankton, Elsevier, 1997.
- [Tomas, H., Ittekkot, V., Osterroht, C. & Schneider, B.: Preferential recycling of nutrients—the ocean’s way to increase new production and to pass nutrient limitation? *Limnol. Oceanogr.* 44, 1999–2004, 1999.](#)
- 1325 Torres, R., Pantoja, S., Harada, N., González, H. E., Daneri, G., Frangopulos, M., ... and Fukasawa, M.: Air-sea CO₂ fluxes along the coast of Chile: From CO₂ outgassing in central northern upwelling waters to CO₂ uptake in southern Patagonian fjords, *Journal of Geophysical Research: Oceans*, 116, C9, doi:10.1029/2010JC006344, 2011.
- Utermöhl, H.: Zur vervollkommnung der quantitativen phytoplankton-methodik: Mit 1 Tabelle und 15 abbildungen im Text und auf 1 Tafel, *Internationale Vereinigung für theoretische und angewandte Limnologie: Mitteilungen*, 9, 1, 1-38, doi:10.1018/05384680.1958.11904091, 1958.
- 1330 [Troupin, C., Machín F., Ouberdous M., Sirjacobs D., Barth A., and Becker J.-M.: High-resolution climatology of the northeast Atlantic using Data-Interpolating Variational Analysis \(Diva\). *J. Geophys. Res.*, 115, C08005, doi:10.1029/2009JC005512, 2010.](#)
- Vanhellemont, Q., and Ruddick, K.: Atmospheric correction of metre-scale optical satellite data for inland and coastal water applications, *Remote sensing of environment*, 216, 586-597, doi:10.1016/j.rse.2018.07.015, 2018.
- 1335 Vaquer-Sunyer, R., and Duarte, C. M.: Thresholds of hypoxia for marine biodiversity, *Proceedings of the National Academy of Sciences*, 105, 40, 15452-15457, doi:10.1073/pnas.0803833105, 2008.
- [Valdenegro, A., Silva, N.: Caracterización oceanográfica física y química de la zona de canales y fiordos australes de Chile entre el estrecho de Magallanes y cabo de Hornos \(CIMAR 3 fiordo\). *Cienc. Tecnol. del Mar* 26 \(2\), 19–60, 2003.](#)
- 1340 Verardo, D. J., Froelich, P. N., and McIntyre, A.: Determination of organic carbon and nitrogen in marine sediments using the Carlo Erba NA-1500 Analyzer, *Deep Sea Research Part A. Oceanographic Research Papers*, 37, 1, 157-165, doi:10.1016/0198-0149(90)90034-S, 1990.
- [Velinsky, D. J., & Fogel, M. L.: Cycling of dissolved and particulate nitrogen and carbon in the Framvaren Fjord, Norway: stable isotopic variations. *Marine Chemistry*, 67\(3-4\), 161–180. doi:10.1016/s0304-4203\(99\)00057-2, 1999.](#)
- 1345 Wang, X., Olsen, L. M., Reitan, K. I., and Olsen, Y.: Discharge of nutrient wastes from salmon farms: environmental effects, and potential for integrated multi-trophic aquaculture, *Aquaculture Environment Interactions*, 2, 3, 267-283, doi:10.3354/aei00044, 2012.
- Williams, P. I., and Robertson, J. E.: Overall planktonic oxygen and carbon dioxide metabolisms: the problem of reconciling observations and calculations of photosynthetic quotients, *Journal of plankton Research*, 13, 153-169, doi:10.1093/oxfordjournals.plankt.a042366, 1991.
- 1350 Yao, W., and Millero, F. J.: The chemistry of the anoxic waters in the Framvaren Fjord, Norway, *Aquatic Geochemistry*, 1, 53-88, 1995.